



USDOT Tier 1
University Transportation Center
on Improving Rail Transportation
Infrastructure Sustainability and Durability

Final Report VT-1

**DETERMINATION OF TOP OF RAIL (TOR) LUBRICITY, USING STATIONARY
AND MOVING CONTACTING AND NON-CONTACTING DEVICES**

By

Mehdi Ahmadian, J. Bernard Jones Chair and Director

and

Dejah Leandra Singh, Graduate Research Assistant

Center for Vehicle Systems and Safety
Railway Technologies Laboratory
Virginia Tech
3103 Commerce Street
Blacksburg, VA 24060

October 31, 2019

Grant Number: 69A3551747132



DISCLAIMER

The contents of this report reflect the views of the authors, who are responsible for the facts and the accuracy of the information presented herein. This document is disseminated in the interest of information exchange. The report is funded, partially or entirely, by a grant from the U.S. Department of Transportation's University Transportation Centers Program. However, the U.S. Government assumes no liability for the contents or use thereof.

ABSTRACT

The examination of the application and accuracy of optical sensors for the purpose of determining rail lubricity of top-of-rail friction modifier is investigated in this research. A literature review of optical sensors as they relate to detecting thin layers is presented, as well as a literature review of the significant aspect of surface roughness on optical signature. Both commercially available optical sensors and optical devices, such as independent lasers and detectors, are examined in a comprehensive parametric study to determine the most suitable configuration for a prototype with adequate third-body detection. A prototype is constructed considering parameters such as sunlight contamination, vibrations, and angle of detection. The prototype is evaluated in a series of laboratory tests with known lubricity conditions for its accuracy of measurements and susceptibility to environmental conditions, in preparation for field testing. Upon field testing the prototype, the data indicates that it is capable of providing subjective measurements that can help with determining whether a rail is highly lubricated or unlubricated, or it is moderately lubricated. It is anticipated that the device could be used to provide a rail lubricity index.

The investigation of the optical response of a rail in various conditions, including top-of-rail friction modifier presence and underlying surface roughness, reveals the behavior of friction modifying material on rail/wheel interactions. It is determined that surface roughness is imperative for distinguishing between scattering due to surface condition and scattering due to third-body layers. Additionally, it is revealed that friction modifying materials become entrapped within the surface roughness of the rail, effectively causing a “seasoning” effect instead of a simple third body layer. This provides some explanation on the inadequacy of determining lubricity conditions using contacting methods since they cannot detect the entrapped material that are revealed only when the top of rail undergoes a micro deformation due to a passing wheel. Furthermore, the fluorescent signature of flange grease can be utilized to detect any flange grease contamination on top of rail. The results of the study indicate that it is possible to have practical optical sensors for top-of-rail third body layer detection and any contamination that may exist, initially through spot checking the rail and eventually through in-motion surveying.

Keywords: Top of rail friction modifier, optical sensors, optical detection, lubric

CONTENTS

DISCLAIMER	ii
ABSTRACT	iii
LIST OF FIGURES	v
LIST OF TABLES	vii
1. Introduction	1
1.1 Motivation	2
1.2 Objectives	4
1.3 Research Approach	4
1.4 Contribution	5
1.5 Report Outline	5
2. Literature Review and Background	7
2.1 Rail Wear and the Importance of Friction Modifiers	7
2.1.1 Failures in Rail/Wheel Contact	7
2.1.2 Lubrication and Friction Modifier Application	8
2.1.3 Benefits of Friction Modifier Use	8
2.1.4 Problems with Lubrication Methods	10
2.2 Background of Optics Sensors	11
2.2.1 Lasers	11
2.2.2 Fluorescence	11
2.2.3 Detectors	11
2.2.4 Filters	13
2.3 Surface Roughness and its Effect on Optical Signature and Rail-Wheel Contact	13
2.3.1 Surface Roughness Definition and Detection	14
2.3.2 Light Scattering Properties	15
2.3.3 Surface Roughness in Rail/Wheel Contacts	16
3. Application of Optics Based Sensors for Lubricity	17
3.1 Previous Field Testing	17
3.1.1 Moving Design Prototype	17
3.1.2 Laboratory Testing for Moving Prototype	19
3.1.3 Field Testing Logistics Summary for Initial Prototype	21
3.1.4 Field Testing Analysis	22
3.2 Parametric Study	26
3.2.1 Beam Spot Size and Location	26
3.2.2 Effects of Ambient Light	28
3.2.3 Angles of Emitter and Receiver	28
3.3 Lubrication Application	30
3.4 Angle Experiments with Top-of-Rail Material	32
3.5 Fluorescence Sensor Testing	38
3.6 Summary of Design Aspects for Prototype	40
3.7 Prototype Design and Capabilities	41
4. Laboratory Evaluation of Prototype Unit	43
4.1 Operation Procedure	43
4.2 Prototype Calibration	44
4.3 Empirical Model for Determining Lubricity	45
4.4 Prototype Experiments with Fluorescence	49

5. Field Testing with Prototype	52
5.1 Testing Logistics	52
5.2 Expectations of Field Testing.....	53
5.3 Test Results	54
5.3.1 Laser Sensor Results.....	54
5.3.2 Fluorescent Sensor Results	59
6. Conclusions and Recommendations	61
6.1 Summary	61
6.2 Significant Findings	61
6.3 Future Studies.....	62
References	63
ACKNOWLEDGEMENTS	65
ABOUT THE AUTHORS	66

LIST OF FIGURES

Figure 1-1: Lubricity optical device constructed for this research, used in laboratory testing (left) and validated through field testing (right).	2
Figure 1-2: Picture of tribometer being used in the rail industry to determine effectiveness of top-of-rail friction modifier material [4].	3
Figure 2-1: Forces acting on train wheelset [5].	7
Figure 2-2: Top-of-Rail lubrication system elements[7].	8
Figure 2-3: Plane wave where lambda represents wavelength [12]	11
Figure 2-4: Two p-n junctions: (a) just formed and (b) on equilibrium, [12].	12
Figure 2-5: Schematic of a p-n junction diode [12].	13
Figure 2-6: Optical Filtering Arrangement [12].	13
Figure 2-7: Diagram of specular and scattered light. (a) is a perfectly reflected beam, demonstrating all specular light and no diffuse light. (b) represents an incident beam on a rough surface, with specular and scattering light.	14
Figure 2-8: Lambertian, or diffuse, scatter of light is governed by a cosine intensity relationship, [17]. ...	15
Figure 3-1: Moving prototype initial design with commercially available and unaltered sensors.	18
Figure 3-2: Keyence NH-32 characteristic diagram, laser emitter and receiver in one fixed unit.	18
Figure 3-3: Balluff 31M characteristic diagram, emitted UV beam and receiver in one unit.	19
Figure 3-4: Comparative readings of two common top-of-rail friction modifiers as a response to laser stimulus from the Keyence laser sensor. These are average readings across the same length of track at approximately the same pushed speed.	20
Figure 3-5: Readings of the same rail condition at different speeds from the Keyence laser sensor.	21
Figure 3-6: Map of testing locations for field testing in 2016 with moving prototype and commercial sensors. Picture was obtained from maps.google.com.	21
Figure 3-7: Response from Keyence laser sensor on the conditioned tangent track during initial field testing. Curves demonstrate 5, 10, 15, and 20mph respective test runs, post-processed data.	23
Figure 3-8: Comparison of the conditioned rail with top-of-rail material (top) and the clean rail section (bottom) for the Keyence laser sensor.	24
Figure 3-9: Response from Balluff fluorescence sensor on the conditioned tangent track during initial field testing. Curves demonstrate 5, 10, 15, and 20mph respective test runs, post-processed data.	25
Figure 3-10: Comparison of the conditioned rail with top-of rail material (top) and the clean rail near a flange grease applicator (bottom) for the Balluff fluorescence sensor.	26
Figure 3-11: Beam spot geometry experiments for parametric study	27
Figure 3-12: Experimental Setup for Keyence Angle Experiments.	29
Figure 3-13: Keyence Sensor Angle Experiments Results	30
Figure 3-14: Separate laser emitter and receiver in-plane experimental setup	33
Figure 3-15: In-plane testing for various top-of-rail materials and thicknesses for a fixed emitter at 45°. Thicknesses are based on shim application.	34
Figure 3-16: Separate laser emitter and receiver for out-of-plane experimental setup.	35
Figure 3-17: Out-of-plane testing for various top-of-rail materials and thicknesses for a fixed emitter at 45°. Thicknesses are based on shim application.	36
Figure 3-18: 3D interpolated response using Matlab. These are the responses for three top-of-rail conditions with a fixed emitter stimulus at 45°.	37
Figure 3-19: Comparison of average readings on Balluff fluorescence sensor as thickness varies for various top-of-rail friction modifiers and flange grease.	39

Figure 3-20: Prototype design, internal structure and user interface.....	42
Figure 4-1: Diagram of box switchboard (left) and controls (right).....	43
Figure 4-2: Kelsan and clean rail test data.....	48
Figure 4-3: Whitmore and clean rail test data.....	48
Figure 4-4: Response of Balluff fluorescence sensor to increasing grease mix with Whitmore top-of-rail material.	49
Figure 4-5: Response of Balluff fluorescence sensor to increasing grease mix with Kelsan top-of-rail material.	50
Figure 4-6: Additional testing of the fluorescent response of Kelsan top-of-rail friction modifier and flange grease (33%).	50
Figure 4-7: Additional testing of the fluorescent response of Whitmore top-of-rail friction modifier and flange grease (33%)	51
Figure 5-1: Map of three locations along Norfolk Southern Rail for field testing in Irons, VA. Picture from maps.google.com.	52
Figure 5-2: Schematic diagram of testing sites (1, 2 and 3), including wayside lubricators. Most traffic is westbound, in this diagram: left to right.	53
Figure 5-3: Field test data overlaid the lab test data for a clean rail and Whitmore top-of-rail friction modifier.....	56
Figure 5-4: Clustered diagram of fluorescent response during field testing.	60

LIST OF TABLES

Figure 1-1: Lubricity optical device constructed for this research, used in laboratory testing (left) and validated through field testing (right).	2
Figure 1-2: Picture of tribometer being used in the rail industry to determine effectiveness of top-of-rail friction modifier material [4].	3
Figure 2-1: Forces acting on train wheelset [5].	7
Figure 2-2: Top-of-Rail lubrication system elements[7].	8
Figure 2-3: Plane wave where lambda represents wavelength [12]	11
Figure 2-4: Two p-n junctions: (a) just formed and (b) on equilibrium, [12].	12
Figure 2-5: Schematic of a p-n junction diode [12].	13
Figure 2-6: Optical Filtering Arrangement [12].	13
Figure 2-7: Diagram of specular and scattered light. (a) is a perfectly reflected beam, demonstrating all specular light and no diffuse light. (b) represents an incident beam on a rough surface, with specular and scattering light.	14
Figure 2-8: Lambertian, or diffuse, scatter of light is governed by a cosine intensity relationship, [17]....	15
Figure 3-1: Moving prototype initial design with commercially available and unaltered sensors.....	18
Figure 3-2: Keyence NH-32 characteristic diagram, laser emitter and receiver in one fixed unit.	18
Figure 3-3: Balluff 31M characteristic diagram, emitted UV beam and receiver in one unit.	19
Figure 3-4: Comparative readings of two common top-of-rail friction modifiers as a response to laser stimulus from the Keyence laser sensor. These are average readings across the same length of track at approximately the same pushed speed.....	20
Figure 3-5: Readings of the same rail condition at different speeds from the Keyence laser sensor.	21
Figure 3-6: Map of testing locations for field testing in 2016 with moving prototype and commercial sensors. Picture was obtained from maps.google.com.	21
Figure 3-7: Response from Keyence laser sensor on the conditioned tangent track during initial field testing. Curves demonstrate 5, 10, 15, and 20mph respective test runs, post-processed data.....	23
Figure 3-8: Comparison of the conditioned rail with top-of-rail material (top) and the clean rail section (bottom) for the Keyence laser sensor.	24
Figure 3-9: Response from Balluff fluorescence sensor on the conditioned tangent track during initial field testing. Curves demonstrate 5, 10, 15, and 20mph respective test runs, post-processed data.	25
Figure 3-10: Comparison of the conditioned rail with top-of rail material (top) and the clean rail near a flange grease applicator (bottom) for the Balluff fluorescence sensor.....	26
Figure 3-11: Beam spot geometry experiments for parametric study	27
Figure 3-12: Experimental Setup for Keyence Angle Experiments.	29
Figure 3-13: Keyence Sensor Angle Experiments Results	30
Figure 3-14: Separate laser emitter and receiver in-plane experimental setup.....	33
Figure 3-15: In-plane testing for various top-of-rail materials and thicknesses for a fixed emitter at 45°. Thicknesses are based on shim application.	34
Figure 3-16: Separate laser emitter and receiver for out-of-plane experimental setup.	35
Figure 3-17: Out-of-plane testing for various top-of-rail materials and thicknesses for a fixed emitter at 45°. Thicknesses are based on shim application.	36
Figure 3-18: 3D interpolated response using Matlab. These are the responses for three top-of-rail conditions with a fixed emitter stimulus at 45°.....	37
Figure 3-19: Comparison of average readings on Balluff fluorescence sensor as thickness varies for various top-of-rail friction modifiers and flange grease.	39

Figure 3-20: Prototype design, internal structure and user interface.....	42
Figure 4-1: Diagram of box switchboard (left) and controls (right).....	43
Figure 4-2: Kelsan and clean rail test data.....	48
Figure 4-3: Whitmore and clean rail test data.....	48
Figure 4-4: Response of Balluff fluorescence sensor to increasing grease mix with Whitmore top-of-rail material.	49
Figure 4-5: Response of Balluff fluorescence sensor to increasing grease mix with Kelsan top-of-rail material.	50
Figure 4-6: Additional testing of the fluorescent response of Kelsan top-of-rail friction modifier and flange grease (33%).	50
Figure 4-7: Additional testing of the fluorescent response of Whitmore top-of-rail friction modifier and flange grease (33%)	51
Figure 5-1: Map of three locations along Norfolk Southern Rail for field testing in Ironto, VA. Picture from maps.google.com.	52
Figure 5-2: Schematic diagram of testing sites (1, 2 and 3), including wayside lubricators. Most traffic is westbound, in this diagram: left to right.	53
Figure 5-3: Field test data overlaid the lab test data for a clean rail and Whitmore top-of-rail friction modifier.....	56
Figure 5-4: Clustered diagram of fluorescent response during field testing.	60

1. Introduction

Optical sensor technology has been an area of research much explored by the rail industry, often utilizing laser technology on various wavelengths. This type of sensor configuration has provided many solutions to the industry, including LIDAR technology for various railway application, including measuring track geometry, curvature, surface condition, and spatial information [1]. In this research, laser technology will be implemented once more in both the visible and ultraviolet light spectrums to qualify the level of lubricity present on top-of-rail. Though optical sensors have been used by the industry for other practices, the application of rail lubricity detection is new. Currently, contacting methods are used to determine the presence, or lack thereof rather, of top-of-rail friction modifier.

The prototype which was designed, constructed, tested, and validated for this purpose measures lubricity using non-contacting methods via laser emission and detection. It allows for a more accurate and reliable means of detection, as laser detectors are capable of distinguishing details at the micro level and do not rely on contacting means which can easily become contaminated or uncalibrated. It also provides a stepping stone for attachment onto maintenance vehicles already implemented in the industry, such as a push cart or hi-rail vehicle. The device constructed takes readings in a stationary manner, where spot checking at various points on a rail is possible. The device is portable and can in theory be used today to answer the question as to whether a rail is adequately conditioned.

The prototype has been calibrated against top-of-rail materials which are used in the industry. Data has been taken under laboratory conditions and that data has been used as reference for determining the level of lubricity at any point which is spot-checked by the prototype. The device will need to be recalibrated if other top-of-rail friction modifiers are used by other organizations.

Because this device was built with the industry in mind, it is fully capable of detecting thin third-body layers at the micron level for the customer who sponsored this project. Its application is immediate and the information which can be obtained by this device can aid the industry in making decisions about lubricator installation or friction modifier material supply, a multi-million dollar expense [2]. As there has been no other reliable way to detect this material or determine if it is effective in various conditions, impact to the industry will be immediate.



Figure 1-1: Lubricity optical device constructed for this research, used in laboratory testing (left) and validated through field testing (right).

1.1 Motivation

The motivation of this research is to design an accurate and reliable means of top-of-rail material detection, which can be easily implemented into industry maintenance practices.

The rail industry works to keep operations safe and reliable, and maintenance costs are significantly considered in all practices and procedures. Regarding rail life, the practice of applying friction modifier and lubricant materials to the top-of-rail and gage of the rail has become standard in recent years since third body layers were beginning to be researched as a means of influencing friction, and therefore, wear [3]. This perspective has shown drastic improvement on rail lifetime, and such friction modifying materials have been researched to achieve optimum levels of the coefficient of friction. The effectiveness of the material as a maintenance operation is well accepted; however, there are no standards for application because this has yet to be determined, as the practice is still relatively new and unresearched. Some companies install wayside lubricators every two miles, others every mile, and this practice can still vary along the same track. Companies spend millions of dollars each year on this practice but are unsure as to whether they are applying too much or too little to optimize cost.

Means of measuring the effectiveness top-of-rail friction modifier are scarce and unreliable. One of the most popular methods is to install strain gauges along the length of the track to measure lateral forces [3]. As friction modifier levels decrease, lateral forces, and consequentially wear, on the rail increase. Locations which demonstrate excessively high lateral forces can be determined to have inadequate friction modifier material present on top-of-rail. However, these gauges are subject to harsh environmental conditions, including extreme temperature differences and thermal expansion, so readings can vary according to environment and season. Additionally, such extreme differences and perpetual expansion and compression limit the life of these gauges dramatically. Frequently they are subject to breaking, and re-installation of these gauges is time consuming, subject to human error, and costly for the industry in lost production time.

Another method of measuring the effectiveness of top-of-rail friction modifier material is through measuring the coefficient of friction using a tribometer [4]. As the goal of the friction modifier material is to mitigate wear on rails caused by excessive forces, regulating the coefficient of friction between the wheel and rail can be a means of determining top-of-rail friction modifier effectiveness. This device is extremely costly and runs very slowly, thus consuming precious operational time for the rail industry. Additionally, as will be discussed later in this paper, this method is inaccurate due to its inability to replicate running conditions as a train wheel passes over the rail. A paper by Jan Lundberg also reports inaccuracy in tribometer measurements [4]. Due to the nature of friction modifier materials becoming entrapped within the surface roughness of the rail, a tribometer cannot effectively access the material and determine accurately the level of lubricity as it lacks the forces required to allow flow of trapped friction modifier material. Additionally, as this research reveals, the third-body layer which can be accessed by contacting means rests on the peaks of the surface roughness of the rail; the friction modifier material on these peaks is only a few microns thick, and as the contacting wheel of the tribometer passes over the material, it becomes contaminated to the point of significantly altering the already thin layer.



Figure 1-2: Picture of tribometer being used in the rail industry to determine effectiveness of top-of-rail friction modifier material [4].

Therefore, it can be determined that contacting methods of measuring such thin and easily altered layers are not as effective as a non-contacting method of measurement. This research will determine the effectiveness of top-of-rail friction modifier not by excessive forces nor by the coefficient of friction, but rather by the presence of the material itself as it appears on the rail. The non-contacting method of determining lubricity conditions on top-of-rail presented in this research is reliable and can be implemented to aid in determining whether or not the industry is utilizing wayside lubricators enough, and if the distance which friction modifier manufacturers claim to carry is accurate in various environmental conditions specific to rail lines. In this way, an optimum balance between cost of lubricity maintenance and cost of rail replacement due to excessive wear can be reached.

1.2 Objectives

This project is centered around answering an industry-based question as to whether or not a particular rail has adequate top-of-rail friction modifier material, particularly using non-contacting methods to do so.

The objectives of this project are to:

1. Devise and test a practical sensor for detecting top-of-rail lubricity for railway application
2. Determine the applicability and effectiveness of optics-based sensors, such as a laser and fluorescence sensor, for qualitative measurement of top-of-rail lubrication
3. Construct a prototype system that can be used for laboratory and field evaluations
4. Use the results of laboratory and field testing to provide recommendations on the feasibility of the technology and a practical system

1.3 Research Approach

The objectives outlined in section 1.2 above are fulfilled through a systematic approach involving the following tasks:

1. Implement an optical sensor configuration which is readily available and test its capabilities to answer if optics-based sensors can be utilized for top-of-rail friction modifier detection
2. Conduct a parametric study to optimize optical sensor characteristics which will most effectively distinguish lubricity conditions
3. Construct a prototype utilizing the optimized characteristics from above which can be used in the laboratory and field alike
4. Develop a numerical calculation specific to the prototype design which can distinguish between adequate and inadequate lubricity conditions for various friction modifiers
5. Conduct field tests at various locations with different lubricity conditions to validate design

Optical sensors proved to be extraordinarily effective in determining lubricity conditions. Though there are many aspects of a surface which can influence its optical signature; once the significant aspects are considered independently, a true detection of lubricity can be determined. This ambiguity is also highly influenced by the level of sensitivity of a sensor, which made an instrument outfitted with completely commercialized sensors unrealistic. This research resolved these issues in the parametric study and in the development of numerical calculations for lubricity measurement.

Using optics-based theory and extensive laboratory experiments, a set of parameters was determined which can take commercial aspects of various instruments and outfit them onto a reliable and relatively inexpensive instrument which is capable of being utilized by industry professionals. This design is effective for the instruments used, and can be further refined with other instrumentation in future designs. The prototype at hand is portable, easy to use, statistically reliable, and ready for practice.

Extensive testing took place with the completed prototype which allowed data to be collected and sorted based on known conditions in the laboratory. From this information, a data set specific to different top-of-rail conditions was collected, against which all field testing data was compared. This data was examined for various influencing factors, surface roughness being key, and empirical calculations were developed to qualify output of various top-of-rail conditions as “adequate” or “inadequate.” This practice assures statistical certainty for readings, allowing a spread between these two qualifying conditions to be developed and examined as well.

Field testing took place with knowledge of the type of conditions present by industry professionals. Knowledge which was used in analysis includes the type of top-of-rail friction modifier used in practice at the testing site, and relative suspected levels of lubricity. The data acquired from this field testing was compared to the laboratory data and it was congruent with the knowledge provided by industry professionals. Therefore, the design of this prototype has been considered verified and effective in achieving the objectives listed in the previous section.

1.4 Contribution

The results of this research have not only answered the industry question of determining lubricity levels, but also revealed several aspects about the interaction of the friction modifier and wheel/rail which can be used to further develop friction modifier materials and measurements devices.

Achieving the objectives of this research consequently provide the industry with a product which is capable of determining accurate levels of lubricity at any location along a rail, regardless of environmental conditions. It can be reconciled with the other measurement devices and aid in calibration for these devices as well.

Constructing this device using non-contacting methods allows growth in design so that the current stationary design can be converted to a moving platform. This would mean that the next iteration of design could potentially be outfitted onto existing maintenance vehicles, such as a hi-rail vehicle, which would decrease loss of production time for this maintenance practice.

Finally, the revelation that top-of-rail friction modifier carries down track and becomes entrapped within the surface roughness of the rail can mean design changes for friction modifier manufacturers. The rail and wheel effectively become “seasoned” with material which is only released upon the next passing train. It also is an aspect which needs to be considered in any future optical analysis of the rail and wheel.

1.5 Report Outline

Chapter 2 presents a literature review relating to all relevant aspects of the research at hand. This includes an explanation as to why the industry requires top-of-rail friction modifier. Additionally, it includes a review on optical devices and theory; specifically, that which was utilized in the construction and analysis of the prototype designed for this research. Finally, it also explores aspects of surface roughness, one of the most significant factors in ambiguity in optical readings.

Chapter 3 provides detail on initial experimentation which justify the end prototype design. This includes initial experimentation with commercially available and unaltered sensors, an extensive parametric study which answered why those commercially available sensors were inadequate for specific and repeatable measurements of lubricity, and design constraints which went into the construction of the final prototype.

Chapter 4 is a laboratory evaluation of the prototype and the development of the basis on which this study justified “adequate” and “inadequate” lubricity levels. A data set was analyzed from known lubricity conditions, and calculations were empirically derived with theoretical inspiration to create a numerical spread of these conditions.

Chapter 5 details the field testing and the following analysis, which verify the design as a practical means of determining lubricity. This summarizes the effectiveness of the prototype and justifies its use as a device which can be used in the industry today.

Chapter 6 provides a summary of all conclusions of this research and explores recommendations for the future of this technology. Because this is the beginning of the application of optics for determining top-of-rail lubricity, there are many ways in which this research can be refined. This chapter details in depth the contributions which were mentioned in the section above.

2. Literature Review and Background

This chapter presents a comprehensive literature review of all relevant information pertaining to this research. It includes the use of friction modifier in the industry, optical theory and background for applicable sensors, and detail on the perspective of surface roughness which this research will adopt.

2.1 Rail Wear and the Importance of Friction Modifiers

This section will detail several aspects of the appropriate rail structure and industry practices as it relates to this study. Material properties and defects of these rail structures must be considered, as the industry seeks to reduce failures. Friction modifier plays an important role in these practices and will be investigated.

2.1.1 Failures in Rail/Wheel Contact

The design and function of a locomotive on a track includes a large locomotive with conical wheels set on a track of a particular gauge. Conical wheels on the locomotive are designed to keep wheels centered on the rail. During normal operations, the contact patch between the wheel and rail will be subject to lateral, vertical, and yaw movement. With this movement comes a set of lateral and longitudinal forces, as seen in Figure 2-1, which causes steering movement but also wear [5].

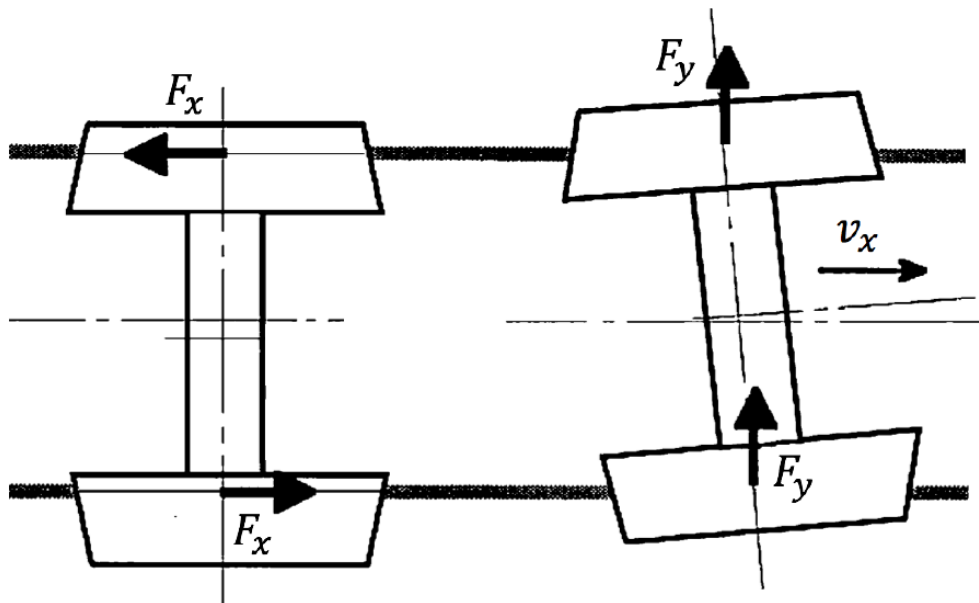


Figure 2-1: Forces acting on train wheelset [5].

These forces contribute to accumulated plastic deformation on the surface of the rails and wheels, commonly referred to as “ratcheting.” Continuous ratcheting as rails and locomotives are in service perpetually cause material deformations, eventually leading to material failure when material ductility is exhausted. Failure of the material is typically begun in the form of micro-cracks, which can grow from continued stress from use or environmental factors. These micro-

cracks propagate from rolling-contact fatigue, or RCF. In an effort to reduce rail and wheel rail wear, RCF is sought to be reduced [6].

There are several preventative practices in the industry to moderate this problem. Rail hardening practices are common to increase the tensile and shear strength of the material, thus increasing the elastic limit, which, when exceeded, causes micro-cracks and RCF [6]. When cracks begin to form, a common maintenance practice in the industry is rail grinding. Rail grinding mechanically removes the top surface of metal from the rail head through rotary grinding stones on a rail car. It takes place either as a corrective measure or a preventative measure [2]. Another preventative measure taken by the rail industry which will be investigated in this study is the application of consumable friction modifier on rails [2]. This will be discussed in the following sections.

2.1.2 Lubrication and Friction Modifier Application

As previously mentioned, lubricants and friction modifiers have been implemented in the industry in an effort to reduce rail/wheel wear for ultimate cost savings. Common application techniques include top-of-rail lubricators, wheel flange lubricators, wayside lubricators, and on-board lubricators [2]. These can be divided into two broad categories of vehicular-mounted lubricators and wayside lubricators, permanently fixed along the track. Traditionally, wayside lubricators are used in the industry, both for friction modifier application and grease lubrication application [5].

Wayside lubricators are activated as a locomotive passes. A computer system applies controlled quantities of top-of-rail material specific to each train. A figure of the elements in this system is shown in Figure 2-2. Data is sent to the system regarding the train's speed, weight, direction of travel, brake pattern, position, track curvature, and ambient conditions. This information is used to dispense the correct and calculated amount of fluid at the appropriate interval during the train's passing [7].

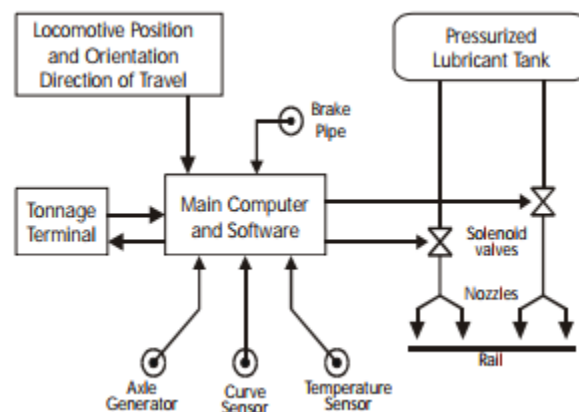


Figure 2-2: Top-of-Rail lubrication system elements [7].

2.1.3 Benefits of Friction Modifier Use

3000 wayside lubricators were installed in Sweden, costing over \$7.9 million according to Waara in a 2000 study. This cost was considered necessary as replacing worn rail is far more expensive, and fuel savings are immediate [2]. Various studies have been completed regarding the application and validity of lubricant and friction modifiers for reducing rail wear. Lubricants aim to reduce friction and are oily in nature, which can actually cause expedited crack propagation as an existing crack is pressurized by these fluids [6]. Friction modifiers on the other hand act as a dry third-body layer, or a dry interfacial layer between the rail and wheel. This layer transmits loads, separates the rail and wheel first bodies, and accommodates differences in speed [3]. The friction modifiers which are supplied from wayside lubricators work with existing third body materials, such as iron oxide composites, to condition the rail and dry, eliminating the crack propagation problem from oily lubricants [3, 8]. Additionally, friction modifiers are designed to moderate the coefficient of friction between the wheel and rail to a specific level, not to simply reduce it [3]. Both lubricants and friction modifiers have appropriate applications; today friction modifier is commonly supplied to top-of-rail, while flange grease lubricant is applied to the gauge face of the rail head. A chart of friction coefficient values accepted by the industry can be seen in Table 2-1 [5].

Table 2-1: Lubrication chart summary [5]

Classification	Coefficient of friction	Description
Dry	0.35 to 0.57	No grease on wear face
Poor	0.30 to 0.35	Lubricant on 10 to 40 percent of the wear face
Acceptable	0.25 to 0.30	Lubricant on 40 to 60 percent of the wear face
Average	0.20 to 0.25	Lubricant on 60 to 90 percent of the wear face
Good	0.15 to 0.20	Lubricant on 100 percent of the wear face
Too much	<0.15	Gauge face and rail head covered by a film of lubricant

Ultimately the application of friction modifier on top-of-rail as a third body has implications in reduction in wear and cost savings. Reduction of contact forces and a decrease in the derailment coefficient as well as an increase in curving performance and decrease in energy consumption are reported by Akira Matsumoto [9]. Reductions in noise, including squeal noise, is reported by Donald Eadie [8, 10]. A decrease in plastic deformation at the surface of the rail, RCF, and rail wear reductions of 30-60% were reported by Donald Eadie as well [6]. Fuel savings have also been a product of friction modifier usage, reported by the US Department of Transportation [7] and S. Kumar [2]. Additionally, the report mentions the lack of negative side-effects friction

modifier has on important parameters such as stopping distance, speed control, or overall handling [7].

2.1.4 Problems with Lubrication Methods

There are several problems with application methods of friction modifier and lubricant today. Excessive lubrication which leaves residue can have harmful environmental effects, and \$2 billion is estimated to be spent in excessive or ineffective lubrication according to the American Association of Railroads. Frequency of lubricators is not standardized, and should be analyzed such that there is a reduction in derailment risk and reduction in rail/wheel wear, while remaining cost effective. Finally, applicator nozzles are frequently in need of cleaning or maintenance, as they have a tendency to clog or function improperly [2].

Two common practices of detecting effectiveness of top-of-rail friction modifier are highly unreliable. One involves the installation of strain gauges along the length of a track, and is considered the most common method of measuring rail/wheel forces in the industry today [11]. These gauges detect small changes in geometry, thus producing strain which is associated with stress for a known material. Excessive strain is associated with excessive forces, particularly lateral forces, which are otherwise mitigated by proper friction modifier application. Therefore, when excessive lateral forces are recorded, it can be concluded that there is inadequate friction modifier material. These gauges are subject to intense environmental conditions, including extreme temperature differences and extreme thermal deformation, which causes these gauges to fail at a relatively frequent rate, and produce ambiguity in reading. The cost of reinstalling these gauges perpetually is ineffective and subject to human error.

A tribometer is an instrument which is capable of measuring the coefficient of friction on a surface. Often they use a spring-loaded wheel with a clutch, where forces are recorded and associated with rolling resistance and slip. These parameters are used to determine the overall coefficient of friction [4]. As friction modifier present on top-of-rail is designed to produce a coefficient of friction in a certain range, a tribometer is designed to detect locations which are out of the desired range, thus indicating the lack of proper friction modifier material present on top-of-rail. However, a tribometer cannot adequately replicate the passing of a locomotive and thus calculates a coefficient of friction which is not accurate. This is due to several factors, including contamination of the wheel as it is perpetually in contact with conditioned rail and is not cleaned between uses, and, as this research will later reveal, that the interaction between the friction modifier and rail/wheel within the surface roughness of the steel cannot be replicated below the elastic limit of the material.

While it is widely accepted that friction modifier in the rail industry has a tremendous cost savings associated with it, both upfront and in preventative measures, there is no consistent way of detecting and inspecting its effectiveness in the field when considering all of the aforementioned issues. Friction modifier in thin films a few microns thick is undetectable to the human eye, and any judgement on its effectiveness is highly subjective. Equipment is limited and the experience of the inspectors plays a heavy role in track inspections [2].

2.2 Background of Optics Sensors

This section will review the optical properties relevant to this study, as well as the physical optical devices implemented. Lasers and detectors will be reviewed in detail, justifying the selection of these devices in the final design, discussed in chapter four.

2.2.1 Lasers

This research and many others incorporate lasers for their consistency in input. A laser has a set direction and is nearly unidirectional in wave characteristic, diverging very little, as seen in Figure 2-3 [12]. The intensity profile is Gaussian, maintaining this profile as it propagates. Properties of lasers which are particularly useful in experimentation demanding consistency include its directionality, monochromaticity, and coherence [5].

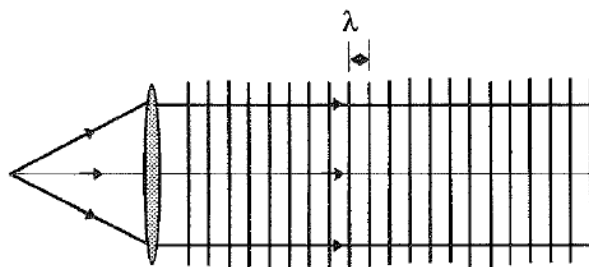


Figure 2-3: Plane wave where lambda represents wavelength [12]

As this beam is used as an input, even its reflection will keep this consistency, which makes it very useful when paired with light detectors fixed to any given surface. Nearly all scattering which takes place will be due to the surface itself, and not inconsistencies with the beam.

2.2.2 Fluorescence

Fluorescence refers to the excitation of atoms and molecules which produce visible light. Ultraviolet light is often used as a stimulus for such a process. The terms “luminescence,” “fluorescence,” and “phosphorescence” all refer to the same phenomenon but have differences in specifying the return to the ground state. Luminescence in present day is one of the most popular methods for chemical analysis and optical sensing. Fluorescence-based sensors are often intensity based, capturing the relationship between a luminophore concentration and the intensity of its emission [13]. Utilizing the fluorescent signature of a substance can be very useful in material identification. Some manufacturers dope materials in fluorescent material to enable adequate and simple detection.

2.2.3 Detectors

There are various types of light detectors which can be utilized in a laboratory setting. Generally, they can be separated into thermal detectors and quantum detectors. Thermal detectors utilize the thermal energy in light rays and the corresponding change in temperature is detected. Quantum detectors are much more abundant in types, including but not limited to photoconductors,

photodiodes, phototransistors, and photomultiplier tubes. The incident light and photon produces electron-hole pairs in the semi-conductor material of the detector which creates the emission of electrons which is detected. Parameters which are considered significant when selecting detectors can be seen and defined in Table 2-2 [12].

Table 2-2: Parameter Identification in Detector Selection [12].

Parameter	Description
Responsivity	Ratio of the output signal to incident intensity ($\mu\text{A}/\text{mW}/\text{cm}^2$)
Detectivity	Ratio of the responsivity to the noise current of the detector itself
Noise Equivalent Power	The reciprocal of Detectivity
Noise	Thermal, shot, or generation-recombination noise
Spectral Response	Variation of responsivity in response to the wavelength
Quantum Efficiency	In photodiodes, the number of electron-hole pairs per incident photon
Frequency Response	Ability to respond to a chopped or modulated beam

Photodiodes are the sensor type selected for this research. They operate off of the simple p-n technology, the pairing of two different materials, p- and n- type, where electrons are dominant in the n-type material and when excited, jump to the hole-dominated p-type material, as shown in Figure 2-4 and Figure 2-5 [12].

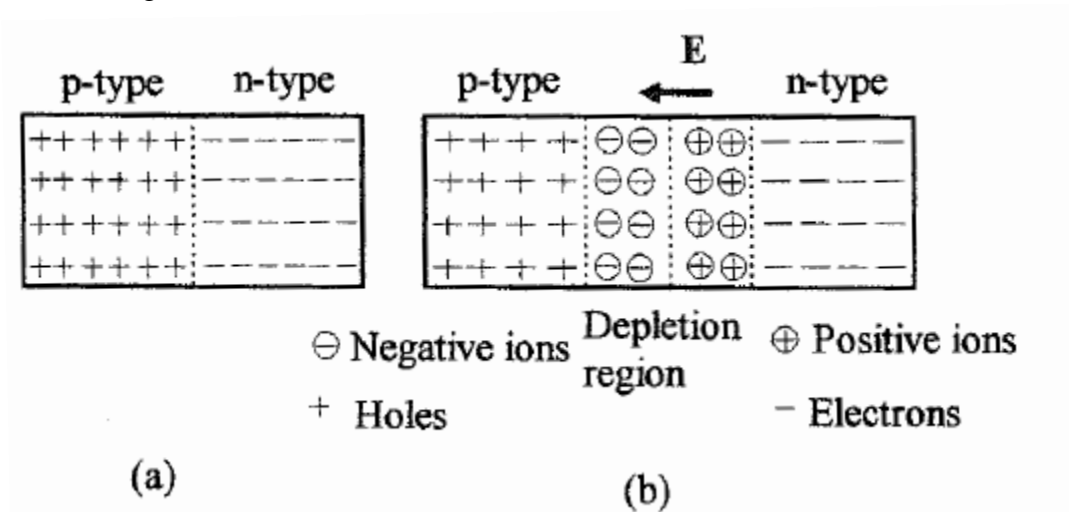


Figure 2-4: Two p-n junctions: (a) just formed and (b) on equilibrium [12].

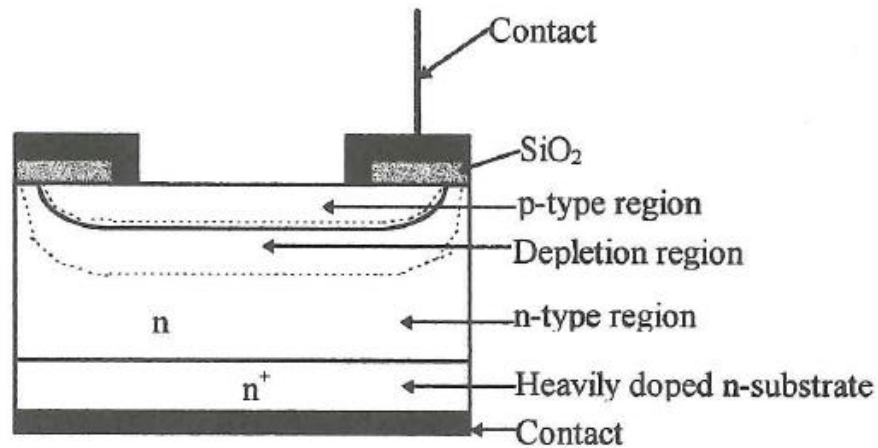


Figure 2-5: Schematic of a p-n junction diode [12].

2.2.4 Filters

Filters are utilized in optics to limit certain frequencies from detection. The physical filter utilizes the mathematics of the Fourier transform, where the zeroth order is shifted by 90 degrees. Effectively, this technology can be used in data processing and image processing alike [12]. A diagram of this phenomenon is shown in Figure 2-6.

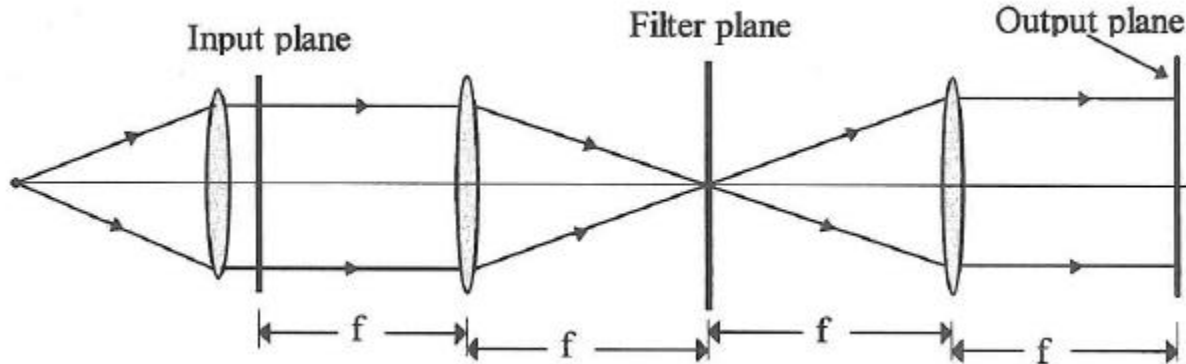


Figure 2-6: Optical Filtering Arrangement [12].

2.3 Surface Roughness and its Effect on Optical Signature and Rail-Wheel Contact

Surface roughness is a physical characteristic which heavily effects the reflectivity of a surface. This study investigates the reflective characteristics of thin films on shiny metallic surfaces, where surface roughness plays a vital role. Considering top-of-rail quality, surface finish can be affected by several different parameters, including degree of rail wear, environmental conditions, material properties of rail steel, and various maintenance practices, such as rail grinding. Because the surface finish can vary widely in the span of a few hundred feet, it is important to separate

reflectivity in the thin film of friction modifier and the surface roughness of the metallic surface underneath.

2.3.1 Surface Roughness Definition and Detection

Surface roughness can be defined in a multitude of ways, but for this paper “surface roughness” will refer to the root-mean-square, or rms, roughness [14]. Other methods of determining surface roughness includes an arithmetic average roughness, which is appropriate if the surface profile is defined as a function. Because this research is highly experimental by nature, the rms definition is more appropriate. This method is one of the most common standards to quantify roughness [14].

After determining the definition of surface roughness for this application, there are several methods which have been utilized to measure this parameter through experimentation. These methods can be divided into two classes: contacting and non-contacting methods. Contacting methods use a physical stylus and measure changes in height along a path. Different stylus tips and implementation methods for contacting profilometers have been investigated and can achieve precision to the level of 10Angstroms and higher [15]. However, the disadvantage of this method is that it cannot be applied easily to moving platforms of higher speeds.

Non-contacting methods are advantageous because they can easily be adopted to a moving platform and can even have higher resolution than the contacting methods [15]. There are a variety of different non-contacting profilers or roughness measuring devices, and the increase in precision comes with the cost of sensitivity and multiple measurements. Lasers are the typical mode of input and scattering is measured from the surface of interest. Some implement a beam splitting design, both incident upon the sample and recollected and compared in height changes. Others do not measure a profile of height changes but rather a more relative roughness, the rms roughness. Often, this involves two separate measurements of the same, unmoved test sample [15].

The principle characteristics of light incident upon a rough surface this study will emphasize is diffuse scattered and specular light. Specular light, equivalent in reflected angle to the incident beam, decreases in intensity as roughness increases while diffuse scattering increases with increasing surface roughness [16]. A diagram of this phenomenon can be seen below in Figure 2-7.

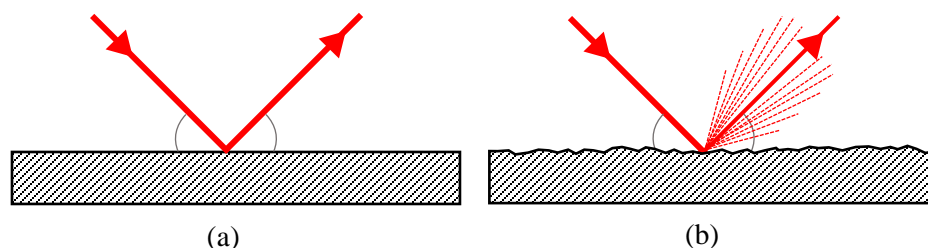


Figure 2-7: Diagram of specular and scattered light. (a) is a perfectly reflected beam, demonstrating all specular light and no diffuse light. (b) represents an incident beam on a rough surface, with specular and scattering light.

2.3.2 Light Scattering Properties

Diffuse scattering can be caused by a variety of different factors, including the material properties of the surface on which light is incident, such as surface finish and reflectivity, and any obstructing materials on the surface, such as thin layered lubricants, polish, or even dust.

Oftentimes in optical calculations, the assumption of a Lambertian surface is made, which is defined to be a surface whose apparent brightness is the same regardless of the angle of observation, especially for diffusing surfaces [14, 17]. This phenomenon is mathematically represented in Lambert's Law in equation (), where intensity is directly proportional to the cosine of the angle of incidence of the beam onto the surface. A figure of this occurrence is below in Figure 2-8.

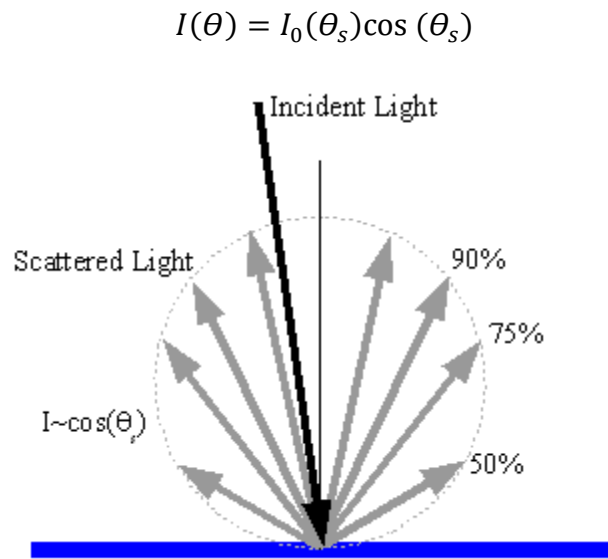


Figure 2-8: Lambertian, or diffuse, scatter of light is governed by a cosine intensity relationship, [17].

Investigating reflective phenomenon can be categorized in two ways: analytically using properties of waves, and geometrically. Wave theory is rooted in physics and utilizes the wave properties of light to quantify and predict changes as they relate to scattering. It is much more mathematically intensive and operates on assumptions of the reflecting surface being a perfect electrical conductor. Though this may be adequate for this application, the latter investigative method is less computationally expensive and defines reflective properties sufficiently. Geometrical optics employ the ray-like behavior of light and is often used to define gross or average characteristics [14]. Most studies referenced in this work investigate the reflective properties of light in a geometrical optics framework.

Within the geometric outlook of scattering, two perspectives can be made to measure scattering as it relates to surface roughness. Total integrated scattering (TIS) compares light reflectance from a single beam, including the specular reflection and all scattered light, measured as a ratio. When put in terms of a TIS detection system and detector output voltage, and equation can be produced,

shown in equation 1, where δ is surface roughness and λ is input beam wavelength [15]. This can be summed up as the fraction of reflected light which cannot be captured due to surface roughness.

$$TIS = \frac{V_{sample, scattered}}{V_{sample, specular+scattered}} = \left(\frac{4\pi\delta}{\lambda}\right)^2 \quad 1$$

Angle resolved scattering (ARS) is the second perspective of the geometric outlook, measured similarly to the TIS method. An ARS instrument is designed to quantify scattering near the reflected specular beam of light, instead of the total scattering [15]. Other configurations blend TIS and ARS methods by measuring near-angle scattering [15].

2.3.3 Surface Roughness in Rail/Wheel Contacts

A relatively unresearched area of study relevant to this paper includes the interaction of the wheel and rail in the train industry at the microstructure level. Surface roughness of the rail itself has been published to range between 5 and 70 microns in magnitude.

In addition to the protection lubricants and friction modifiers have on rail and wheel wear, surface roughness can serve as another mode of protection. Referring to material science theory, when loads exceed the elastic limit, the corresponding plastic deformation results in residual stresses and strain hardening. This is a process which can be used to strengthen a material, enabling it to support loads higher than the material's natural elastic limit allows [18]. Because the rail and wheel make contact at asperities defined by the surface roughness of the material, contact pressures at these points are much higher than at an average pressure. These asperities therefore are subject to plastic deformation as the elastic limit is exceeded, enabling the strain hardening process to occur at the microstructure level within a few microns of the surface of the rail.

This research is still under development, both in experimentation and models. Christoph Tomberger [19] created a model which can include the interaction of friction modifiers and lubricants on the rail while considering asperities and surface roughness, and several studies have been conducted which demonstrate increased contact pressure at the surface of a rough material [18]. Even still, this field needs to be investigated further with validation through experimentation from lab experimentation and field tests of realistic contact pressures and lubrication conditions.

3. Application of Optics Based Sensors for Lubricity

Though the optical theory and instrumentation discussed in chapter two has many applications, this project will apply optical technology to the detection of thin layer friction modifier on a shiny metal rail of a particular surface roughness. This chapter will detail several factors independently considered which went into the selection of the optimal instrument design, including initial experimentation with commercially available instruments, and also report a parametric study and calibration experiments based on the failures of these commercially available instruments. The conclusions from these studies will be summarized and details about the prototype design will be outlined. The nature of these experiments are highly empirical in nature, with aid from optical theory.

3.1 Previous Field Testing

Early in 2016, a moving prototype was designed and constructed using a Keyence NH-32 Laser and a Baluff 31M sensor for speeds in the walking range and for a hi-rail vehicle. This section will detail the design aspects, field testing logistics, and evaluate how this prototype performed in the field with unaltered and commercially available instruments. This section will justify the need for a re-examination of the sensor configuration for such a prototype, which will lead to a parametric study of sensor characteristics following this field testing.

3.1.1 Moving Design Prototype

An initial prototype was designed and equipped with two sensors which examine the top-of-rail for lubricity conditions, and supporting instrumentation which makes the prototype capable of movement. This includes a data acquisition system, speed actuator, and GPS capability. It was designed to be capable of recording both at walking speeds and attached to a hi-rail vehicle. A figure and picture of these configurations can be seen in Figure 3-1 below.

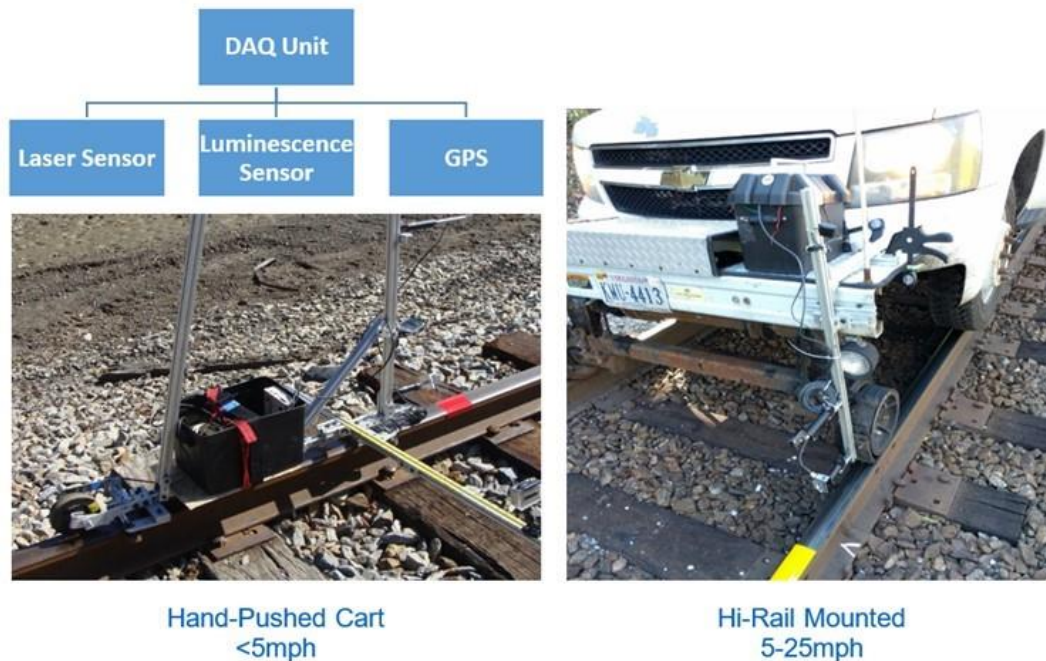


Figure 3-1: Moving prototype initial design with commercially available and unaltered sensors.

Both sensors are an all-in-one design, where both the emitter and receiver are fixed and offset by a few degrees within the sensor housing. A diagram of the Keyence laser sensor and the Balluff luminescence sensor can be seen in Figure 3-2 and Figure 3-3 below.

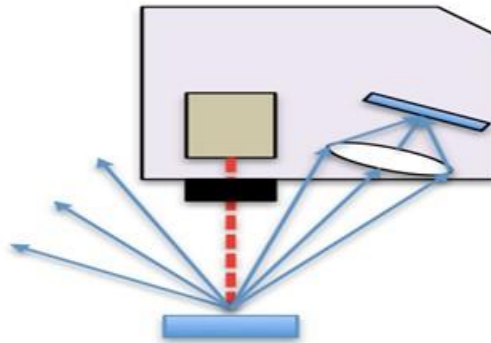


Figure 3-2: Keyence NH-32 characteristic diagram, laser emitter and receiver in one fixed unit.

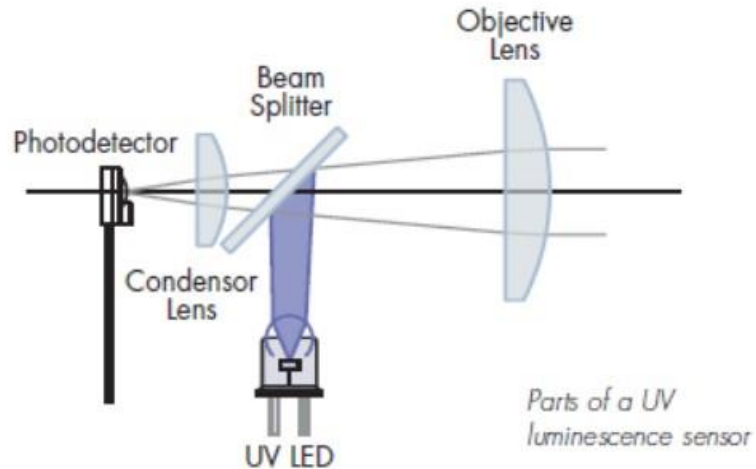


Figure 3-3: Balluff 31M characteristic diagram, emitted UV beam and receiver in one unit.

The GPS unit was installed to track the location of the prototype on the rail, including velocity data. Speed was also recorded through a rotary sensor configured on the wheel of the prototype. All data was recorded and stored in a DataQ Instruments model DI 710-ULS.

3.1.2 Laboratory Testing for Moving Prototype

This unit proved to be successful in overall detection of different conditions in a laboratory environment. This includes low speed movement and known applied conditions. The unit was tested to identify conditions in comparison to a clean or dry rail. Figure 3-4 represents the response of this laser on average when pushed at low and relatively consistent speeds. It can be seen that there is indeed a substantial detection of different top-of-rail conditions for a repeated type of track. Furthermore, testing showed consistency in readings as speed varied, achieving percent error of 0.9%, as shown in Figure 3-5.

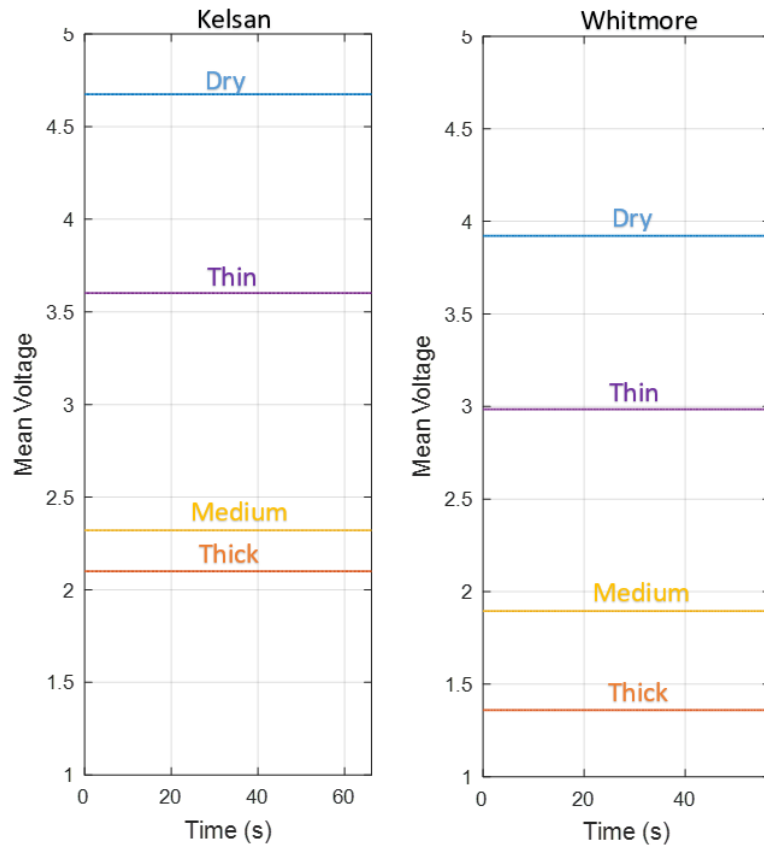


Figure 3-4: Comparative readings of two common top-of-rail friction modifiers as a response to laser stimulus from the Keyence laser sensor. These are average readings across the same length of track at approximately the same pushed speed.

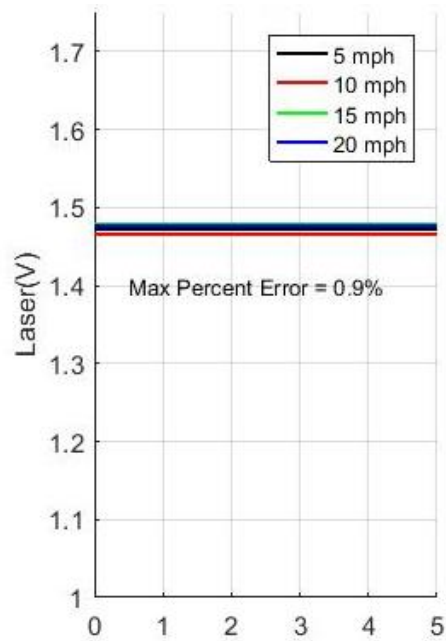


Figure 3-5: Readings of the same rail condition at different speeds from the Keyence laser sensor.

3.1.3 Field Testing Logistics Summary for Initial Prototype

Field testing took place in Ironto, Virginia with the sponsorship of Norfolk Southern. The unit was tested at two separate locations: a curve and tangent track. The map view of these two locations can be seen in red outline in Figure 3-6 below.



Figure 3-6: Map of testing locations for field testing in 2016 with moving prototype and commercial sensors. Picture was obtained from maps.google.com.

Data was taken on the hi-rail only in both cases. There was a grease applicator located approximately 500 feet east of the curved track, and a top-of-rail applicator approximately 200

feet east of the testing location. Traffic on this rail is heavily east-west. 150 feet of track for both sections were tested for several test runs. Reflective tape of red color and six inches in length was placed every 75 feet to track as an indicator of the beginning, middle, and end of each run. Hi-rail tests were completed at 10, 15, and 20 miles per hour across the same stretch of rail.

3.1.4 Field Testing Analysis

The completion of this field test validated the sensitivity laser and fluorescence detectors have in being able to detect third body layers on top-of-rail, but were ambiguous in overall magnitude of readings. The successes were marked by consistent readings of the laser sensor in reading surface figure of the rail regardless of speed. **Error! Reference source not found.** demonstrates the consistent laser response on the conditioned tangent track after data processing. Note the similarity in peak structure, illustrating consistency in readings along the same track. Line averages were taken across each curve to demonstrate overall curve behavior. The first two equations for 5 and 10mph speeds are nearly identical in slope and intercept. The 15 and 20 mph runs change slightly and adopt a slightly negative slope. This is believed to be a result of contamination of the track as test runs were repeated, and also due to the very narrow band of sensitivity this particular sensor provided given the slight change in speed and environmental conditions.

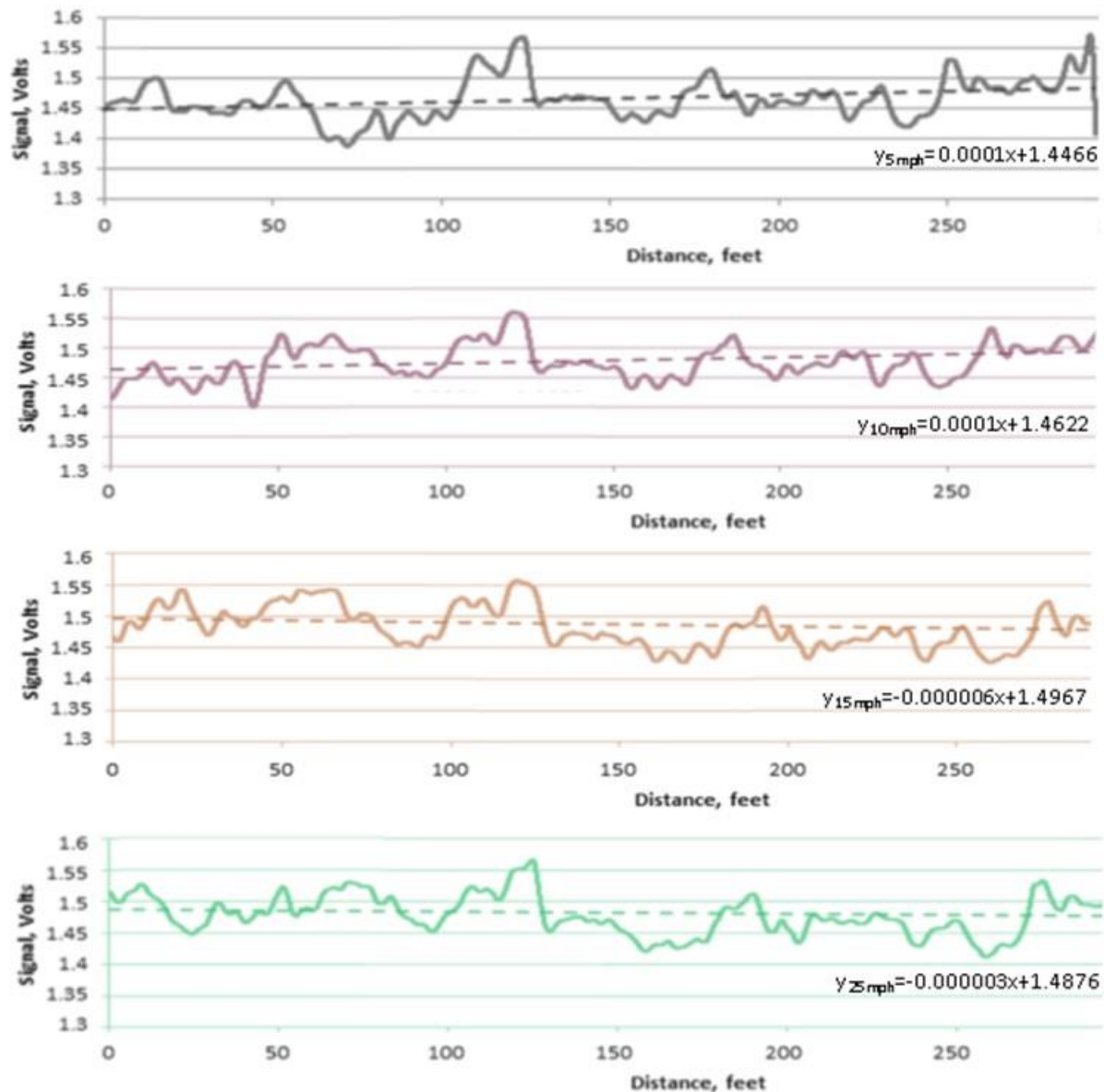


Figure 3-7: Response from Keyence laser sensor on the conditioned tangent track during initial field testing. Curves demonstrate 5, 10, 15, and 20mph respective test runs, post-processed data.

There were several shortcomings of this sensor which were also revealed in this field testing. There was a high level of variance which appeared reasonable in laboratory conditions but not in field testing. Variance was caused by vibration of the sensor as the vehicle moved, creating a level of uncertainty which was not acceptable to distinguish conditions in such a sensitive and narrow band. Additionally, the variance caused by the surface roughness alone was too high to distinguish between different lubricity conditions. The consistency in peak location between the curves above demonstrate the effect of surface roughness, which was highly influential on readings, rendering response data useless when another section of track is considered. Figure 3-8 shows the drastic difference in response data from the above conditioned section of track and the more dry curved section of rail. Though there is success in the overall behavior when considering the line of best

fit which was resolved, it reveals much more inconsistency and ambiguity in readings. It is expected that the dry section has an increase in response due to the increase in specular and near-specular light reflected from the shinier rail surface. However, because the peaks do not match, it is impossible to distinguish between readings being a result of surface finish or true change in lubricity conditions.

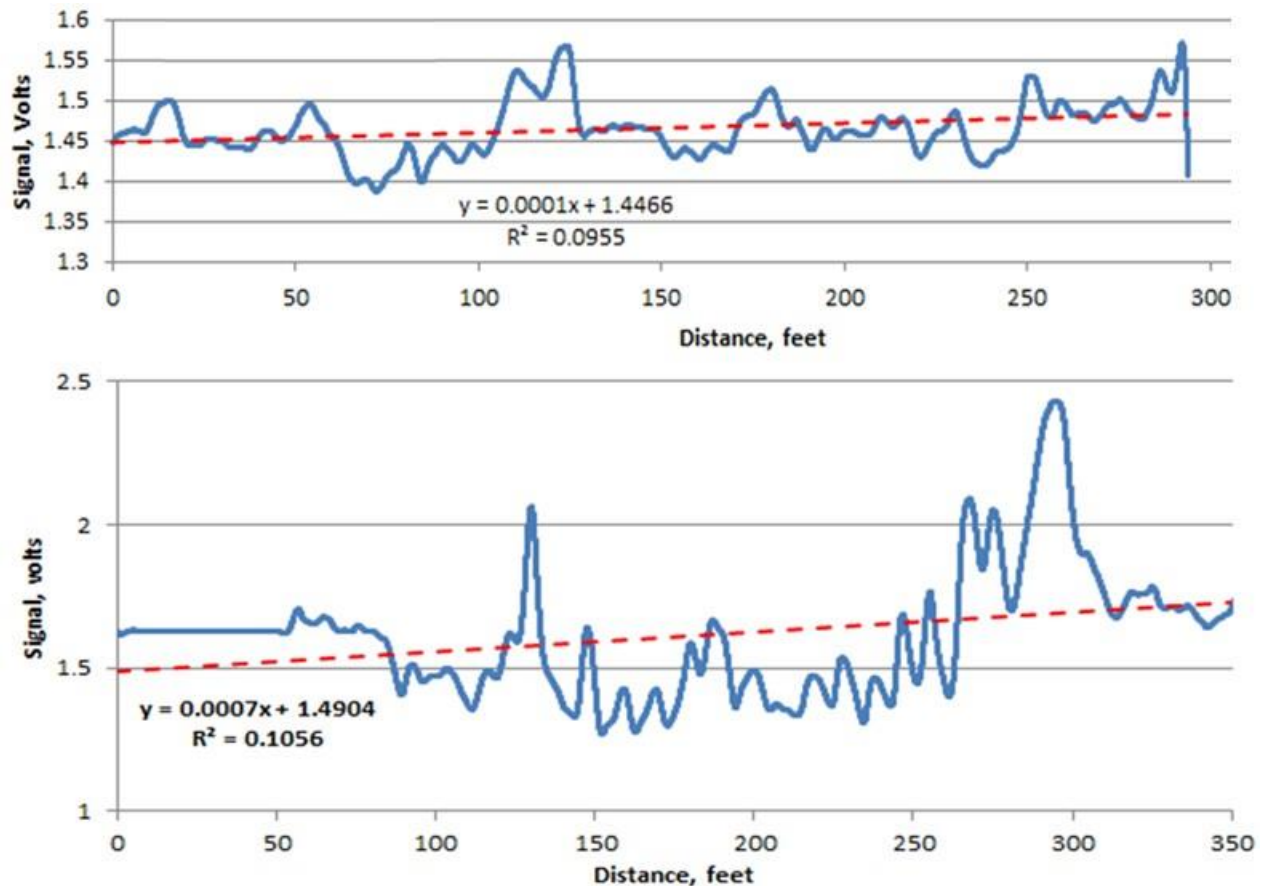


Figure 3-8: Comparison of the conditioned rail with top-of-rail material (top) and the clean rail section (bottom) for the Keyence laser sensor.

Fluorescent data using the Balluff sensor was very similar in result to the laser data after being processed, as seen in Figure 3-9. The various runs at different speeds were more or less consistent, especially in curve shape. Overall trend lines demonstrate coherence as well, though they vary in approximately the same manner and degree as the trendlines for the laser data. Perhaps this is due to the contamination of the rail or increased vibration and therefore variance as the vehicle increases speed, thus creating these small changes which were not clear in the lab data.

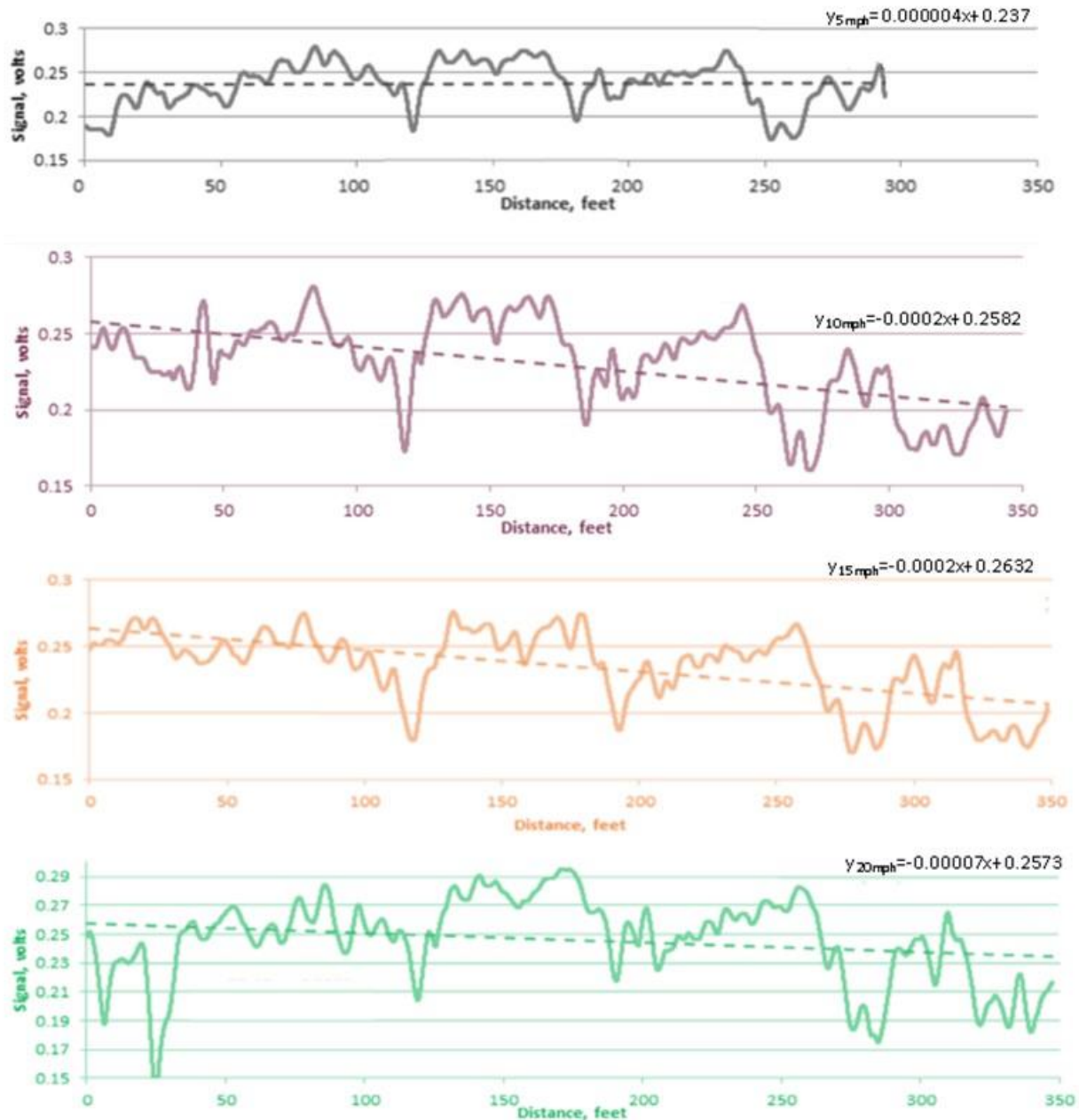


Figure 3-9: Response from Balluff fluorescence sensor on the conditioned tangent track during initial field testing. Curves demonstrate 5, 10, 15, and 20mph respective test runs, post-processed data.

Again, the fluorescent sensor demonstrates the inability to distinguish readings on a different section of rail. When comparing the clean, dry section of rail to the conditioned rail in Figure 3-10, variance becomes very high. However, overall analysis of magnitude seems to be consistent with predictions; as the “dry” section of rail was closer to the grease applicator and therefore would likely have more flange grease contamination, readings were expected to be higher here and they are marginally. It is unclear if this is simply an artifact of the environment, however.

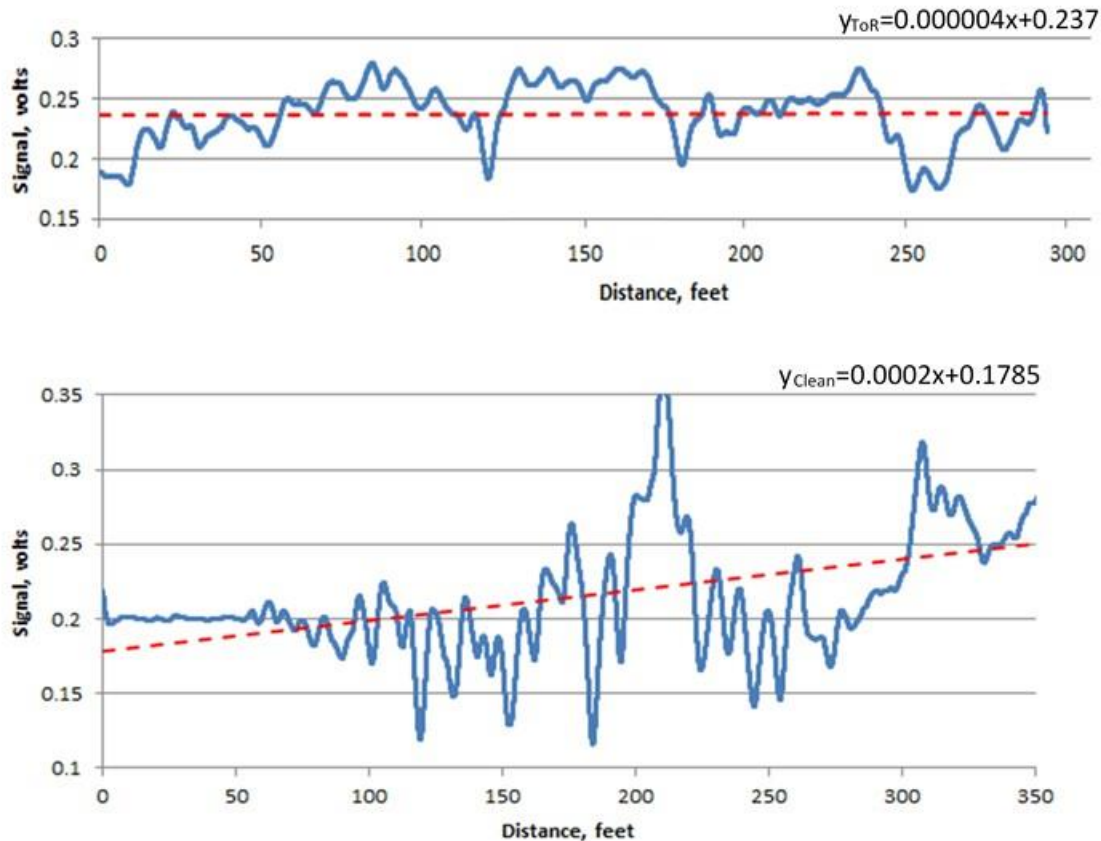


Figure 3-10: Comparison of the conditioned rail with top-of rail material (top) and the clean rail near a flange grease applicator (bottom) for the Balluff fluorescence sensor.

Overall, this round of field testing demonstrated that the optical configuration with lasers is sensitive enough to distinguish various top-of-rail conditions, but is shrouded in ambiguity from many different factors. The next phase of the project was to experiment with each potential source of ambiguity in readings and design a new prototype which eliminated as much ambiguity as possible.

3.2 Parametric Study

A parametric study was conducted where a series of experiments with one independent variable was piloted. Each subsection will detail the experimental design and conclusions from each parameter.

3.2.1 Beam Spot Size and Location

As the objective of this study is to determine lubricity for top-of-rail material, the area of the rail of primary concern is along the tapeline. As a train passes, conical wheels are centered in one area along the rail, which is referred to here as the tapeline. The conical wheels are constantly “hunting” along this patch, as it spans about an inch and a half in the center of the rail head. The focus here

was to see if there were significant differences in readings as the location was changed within this tapeline, and if size and geometry of the beam were significant in contributing to readings.

For the first set of experiments in this section, a collimated and focused beam were compared. On an optical bench, five points were examined on the same rail sample with no lubricant or friction modifier applied, 2.5mm from the center point. The distribution of points can be seen in Figure 3-11. All data was taken in a light-controlled setting within a dark box. A Keyence LV-NH32 laser sensor was used and set perpendicular to the rail tapeline at a 375mm stand-off height. The dynamic range for this particular sensor is 1V-5V.

Averages and standard deviations reflect the precision of the sensor, and Table 3-1 shows the results of these experiments. The readings vary significantly according to an ANOVA test conducted at 95% confidence levels. This reveals that the sensor is sensitive to these two parameters of beam geometry and location. Though the focused beam is more precise, the collimated beam is desirable for this application because the focus is not within a pinpoint, but rather on an average over a spot. The focused beam is much more sensitive to surface roughness while the collimated beam can take more of an average of a larger spot, revealing overall surface characteristics. Another point to mention is that the sensor was unable to capture the true difference in the bottom spot location because the signal became saturated at this point, thus the information was lost.

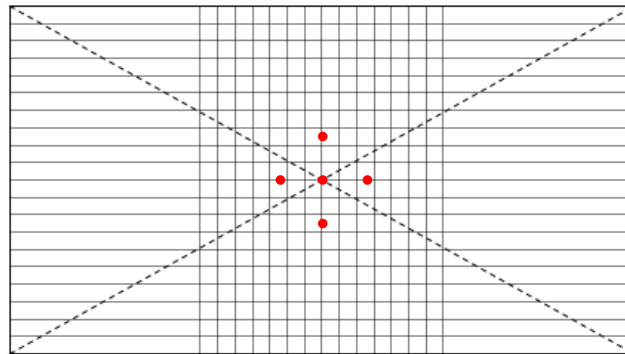


Figure 3-11: Beam spot geometry experiments for parametric study

Table 3-1: Collimated vs Focused averaged data for Keyence laser sensor examination in beam spot influence.

	Average		Standard Deviation	
	Focused	Collimated	Focused	Collimated
Center	4.737766529	4.816696069	0.021399143	0.022695923
Right	4.526808083	4.969575712	0.021655046	0.021471464
Left	4.739023338	4.787890562	0.022650124	0.022417714
Top	3.956269248	3.516594513	0.021591823	0.021373825
Bottom	4.970709359	4.970276577	0.021603278	0.021189877

3.2.2 Effects of Ambient Light

Experimentation was also done to capture the effects of ambient light for this configuration as well. The same experimental setup was upheld as in section 3.2.1 regarding the rail condition, sensor and data acquisition configuration, and five spot geometry testing. The lighting conditions were varied from dark, which was within a closed box, and light, which was supplied from ambient light from a laboratory.

Again, averages and standard deviations reflect the precision of this sensor, and Table 3-2 shows the results of these experiments. Again, the readings vary significantly according to an ANOVA test conducted at 95% confidence levels. This reveals that the sensor is sensitive to ambient light. Though the differences in readings aren't large, it creates a point of ambiguity in different top-of-rail conditions within the deviation of readings of known conditions previously demonstrated in initial testing with commercial sensors. Again as well, the sensor saturated in the bottom condition, making the true difference in readings impossible to tell. For best practice, eliminating any ambiguity caused by ambient light would produce most consistent results.

Table 3-2: Ambient Light experiments for parametric study

	Average		Standard Deviation	
	Dark	Light	Dark	Light
Center	4.816696	4.968763	0.022696	0.02251
Right	4.969576	4.847447	0.021471	0.023238
Left	4.787891	4.895509	0.022418	0.025136
Top	3.516595	3.53731	0.021374	0.022128
Bottom	4.970277	4.96817	0.02119	0.022198

3.2.3 Angles of Emitter and Receiver

Because the sensor used for the above investigations had a fixed emitter and receiver within one unit, experiments were done exploring both the effects of this particular sensor at different angles and of another sensor where the emitter and receiver were separate units. The offset within the Keyence sensor is about 4°, capturing near specular and back-scattered light when placed normal to the surface of interest. This section will cover the angle experiments done with the Keyence sensor only, as the latter will be discussed further in this chapter.

Experimentation was also done to capture the effects of ambient light for this configuration as well. The same experimental setup was upheld as in section 3.1.1 and 3.1.2 regarding the rail condition, sensor and data acquisition configuration, and five spot geometry testing, adjusting the stand-off height to 250mm for practical considerations. Ambient lighting was consistent as all testing was completed within the dark box. The angle of incidence was varied longitudinally along the rail in increments of one degree, ranging from -8° to +8°. A picture of this experimental setup can be seen in Figure 3-12.

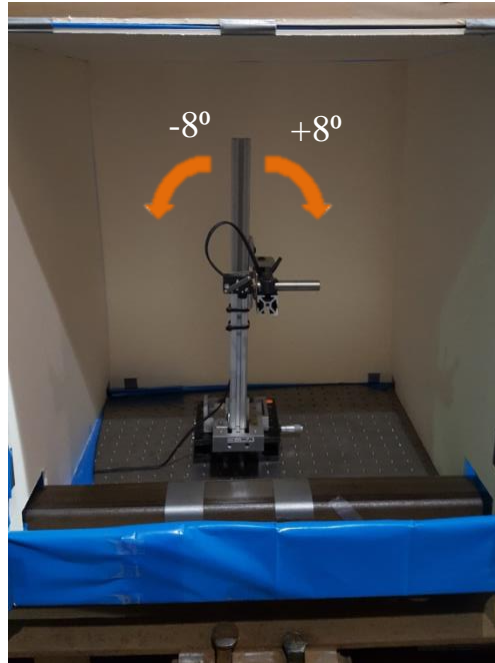


Figure 3-12: Experimental Setup for Keyence Angle Experiments.

Results of these experiments can be seen in

Figure 3-13. Each of the five points are displayed as angle is varied along the x-axis, and an average of the five points is also recorded for overall behavior at a particular angle. The largest problem with this sensor which was demonstrated was its very narrow band of dynamic range. In order to be within the 1-5V limit, the sensor had to be oriented from -7° to -3° and $+3^\circ$ to $+7^\circ$ to avoid saturation. Directly normal to the rail surface risked saturation, as seen in this experiment as well as the experiments detailed previously in this chapter. This sensor was so sensitive to angle that precise and repeatable readings will also be ambiguous if even the configuration changed marginally. Therefore, this sensor cannot be used on a moving platform for risk of vibration and alteration of signal calibration levels. In order to slightly increase its dynamic range, stand-off height could be increased so that saturation doesn't occur as quickly, but the tradeoff is that a larger stand-off height would be more sensitive to vibration and cause more ambiguity. This series of experiments pointed toward the need for a separate emitter and receiver to best capture proper scattering profiles. The results of this experiment also pointed toward the need for a stationary device.

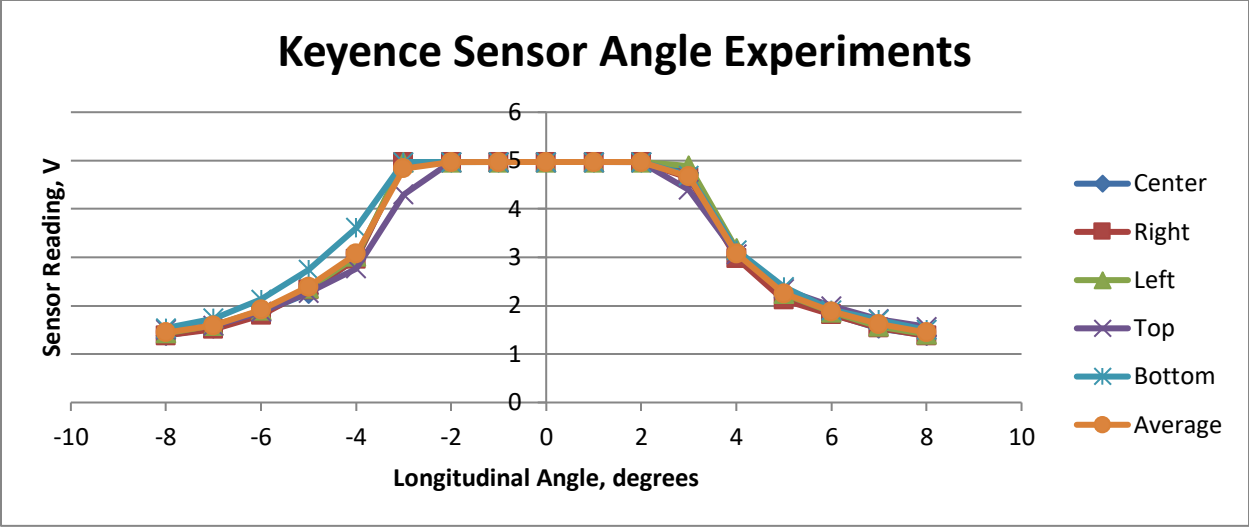


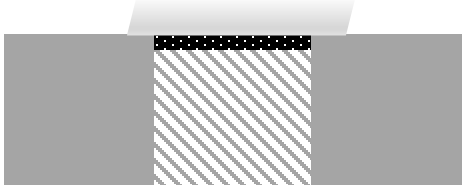
Figure 3-13: Keyence Sensor Angle Experiments Results

3.3 Lubrication Application

A method of known application of top-of-rail material is required in order to successfully calibrate a device to correctly identify both type and relative thickness of various materials. Measuring thin layers at the order of micrometers while in the liquid state is challenging. For this project, metal shims of known thicknesses were implemented to apply a calibrated and known thickness to rail samples in the lab. Stainless steel shims were cut to 10μm thicknesses and layered to create 10, 20, and 30μm thicknesses; an additional steel shim of 25μm thickness was implemented for initial testing as well. The shims were fastened to the rail about 1-2” apart from each other, leaving a cavity of rail between the shims. Top-of-rail material was applied in excess between the shims and scraped off using a microscope slide along the curvature of the rail. Table 3-3 demonstrates the application process. In this way, liquid material was applied to the rail in repeatable thicknesses.

Table 3-3: Chart of Application Process of Top-of-Rail Material

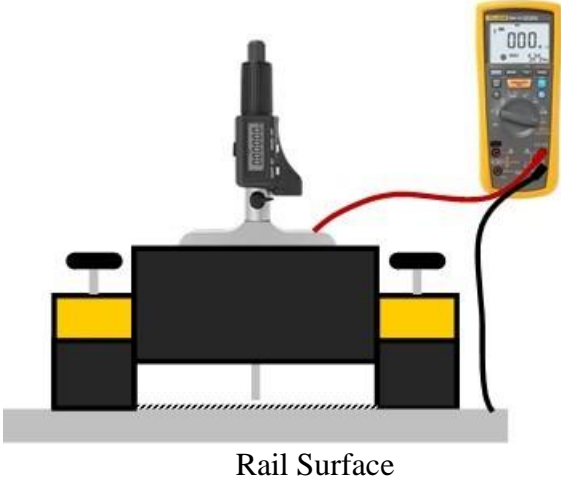
Diagram of Setup	Description of Process
	Two shims (grey) are applied on either side of a patch of clean rail (lined surface). Shims can be layered to produce various thickness levels.
	Top-of-Rail material (black spotted) is applied in excess on rail surface.

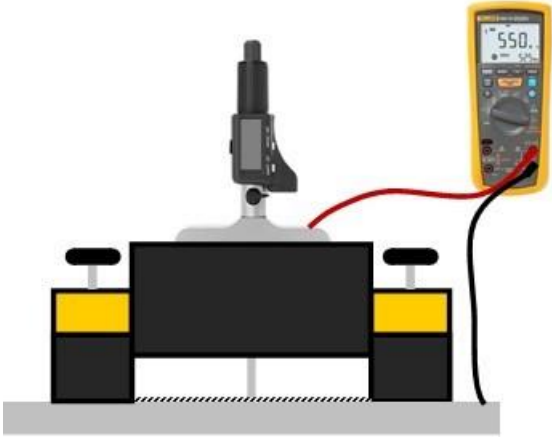
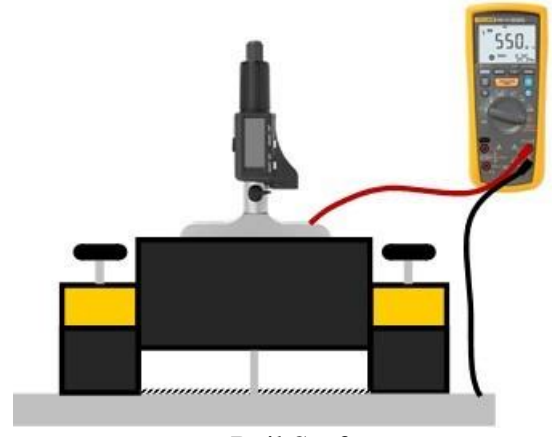
	<p>Excess material is scraped away using a microscope slide (grey gradient), in and out of the page in this diagram, so that the remaining thickness matches that of the shim thickness.</p>
---	--

Despite uncertainty in actual thickness of material, this method provides a repeatable thickness to be applied in future experimental studies.

An additional instrument was utilized which was designed and fabricated in the Center for Vehicle Systems and Safety by Dr. Andrew Peterson. This instrument capitalizes on the conductive nature of Top-of-Rail material as a depth micrometer slowly makes contact with the Top-of-Rail material and then the steel rail, respectively. A figure of this process can be seen in **Error! Reference source not found..** Using this instrument, it would found that the thicknesses applied using the shim method were not accurate to the thicknesses of the shims themselves, but still provided a means of consistent and repeatable lab testing.

Table 3 4: CVeSS Thickness Instrument Diagram

Diagram of Setup	Description of Process
 <p style="text-align: center;">Rail Surface</p>	<p>Micrometer is fixed to the rail using magnetic fasteners. The micrometer and rail surface are connected to a high resistance ohm-meter or multi-meter. Micrometer is slowly incremented from empty space while the multi-meter reads “infinite” ohms or no connection.</p>

 <p style="text-align: center;">Rail Surface</p>	<p>Micrometer makes contact with the ToR material at one instance. At this point, there will be a reading for resistance as a weak connection has been made between the multi-meter and the rail through the third body material. A depth is recorded at this point as well.</p>
 <p style="text-align: center;">Rail Surface</p>	<p>Micrometer continues to increment until internal clutch is activated, thus bottoming out the micrometer on the rail surface. A depth is recorded at this point. The two recorded depths are subtracted for a total thickness of top-of-rail material.</p>

3.4 Angle Experiments with Top-of-Rail Material

One goal of this project was to gather information about the light characteristics each top-of-rail material demonstrated under laser stimulus. Angles of both the emitting laser and receiving detector were varied to determine a lobe-like response for each stimulus. Additionally, this set of experiments explored the industry-used method of observing material on top-of-rail from a grazing angle (close to 90° from the vertical).

For the first set of angle experiments with top-of-rail material, the laser was fixed at either a 0° , -30° , -45° , -60° , or -75° angle from the vertical, in line with the rail length, as seen in

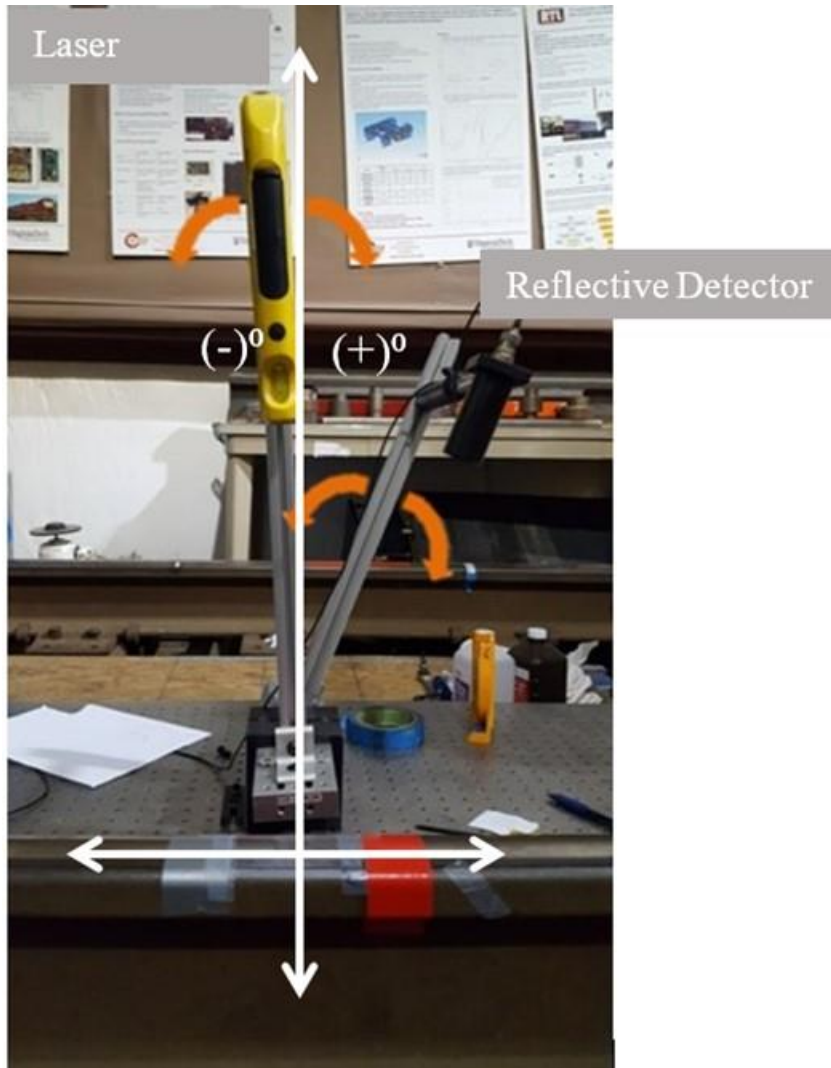


Figure 3-14. The corresponding detector moved from 15° from the emitting laser position down to the grazing angle in 15° increments. For example, a fixed laser emitter at -60° to the vertical axis would have detector readings at -45° , -30° , -15° , 0° , 15° , 30° , 45° , 60° , 75° , and 90° , ranging from backscatter to forward scatter and grazing angles and including specular reflection. All experiments were done in the dark, executed by covered windows and lights turned off within the laboratory.

Special care was taken to ensure the point of rotation for these experiments maintained the same laser spot position. Readings were taken live and recorded by hand, measured in watts. In-plane testing was completed for clean rail conditions in addition to one, two, or three layer shim thicknesses of the available top-of-rail material provided by the corporate sponsor. For initial testing, this included Kelsan Winter, Whitmore Armor, and flange grease products. All readings were taken on the same rail sample in the same approximate location.

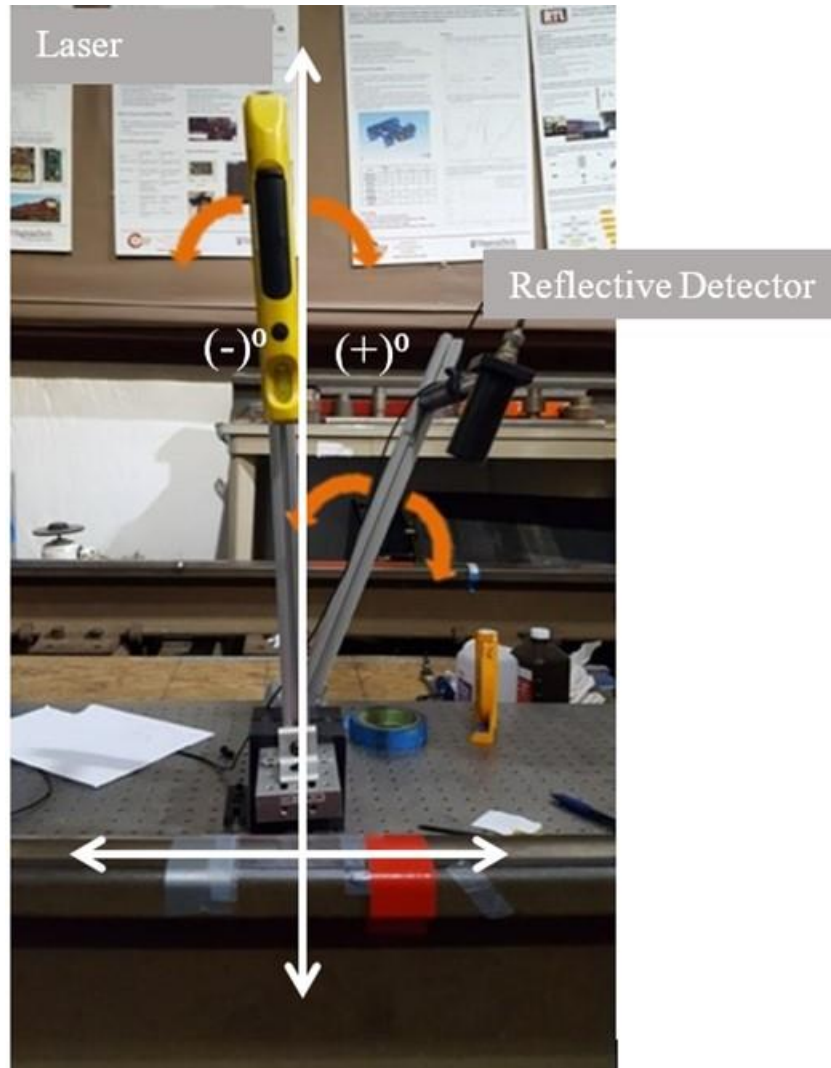


Figure 3-14: Separate laser emitter and receiver in-plane experimental setup

A sample response of in-plane experimentation can be seen in Figure 3-15. In this plot, the response of several top-of-rail materials are demonstrated while stimulated by a laser at one fixed angle. In this example, the laser is fixed at 45° while the receiver sweeps from -30° (backscatter) to 90° (forward scatter) in 15° increments. The measurements taken have been displayed on a log plot due to the difference in magnitude of the specular response in relation to the scattering response.

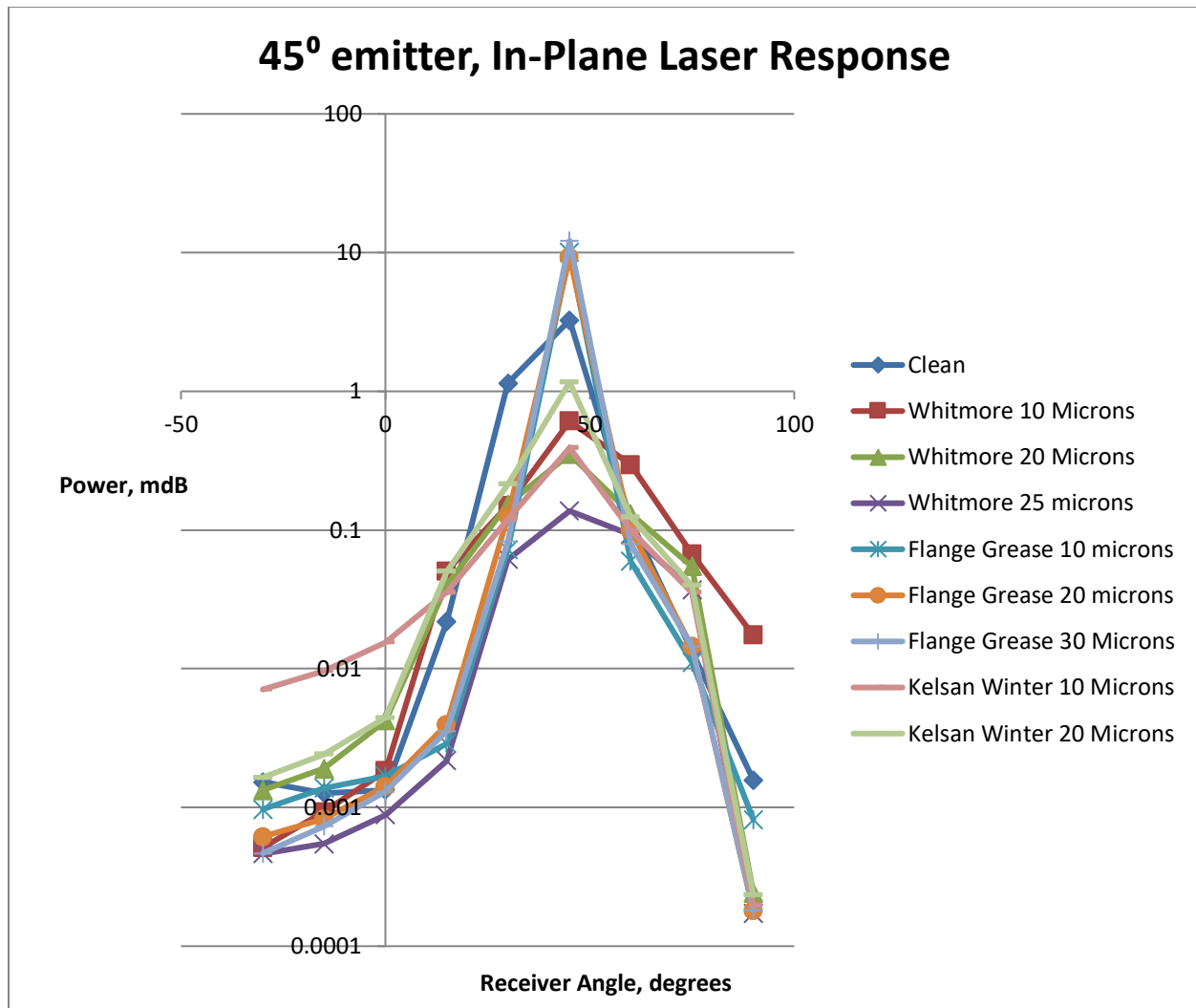


Figure 3-15: In-plane testing for various top-of-rail materials and thicknesses for a fixed emitter at 45°. Thicknesses are based on shim application.

Not only were in-plane measurements important to study, but out-of-plane measurements allowed a full 3D spliced view of the light response a material had to a laser stimulus. Out-of-plane measurements removed any effects of speckle from the detector and demonstrate the width of light response a material had.



Figure 3-16 shows the experimental setup for out-of-plane measurements. Ambient light and other experimentation logistics were maintained from in-plane experimentation. The emitter included 0° , -30° , -45° , -60° , and -75° increments. Receiver sweeping angle increments consistently ranged from -45° to 90° for the receiver, except for when the emitter fixed directly normal to the rail. These movements were restricted by the physical parameters of the setup.



Figure 3-16: Separate laser emitter and receiver for out-of-plane experimental setup.

A sample of the response in these tests is shown in Figure 3-17. These were developed for each top-of-rail material on hand, and at various thicknesses using the aforementioned shim application method. All testing was completed on the same rail sample at approximately the same location. A log plot of this data was not necessary as there was no single point which dwarfed all other readings as the specular did in in-plane testing.

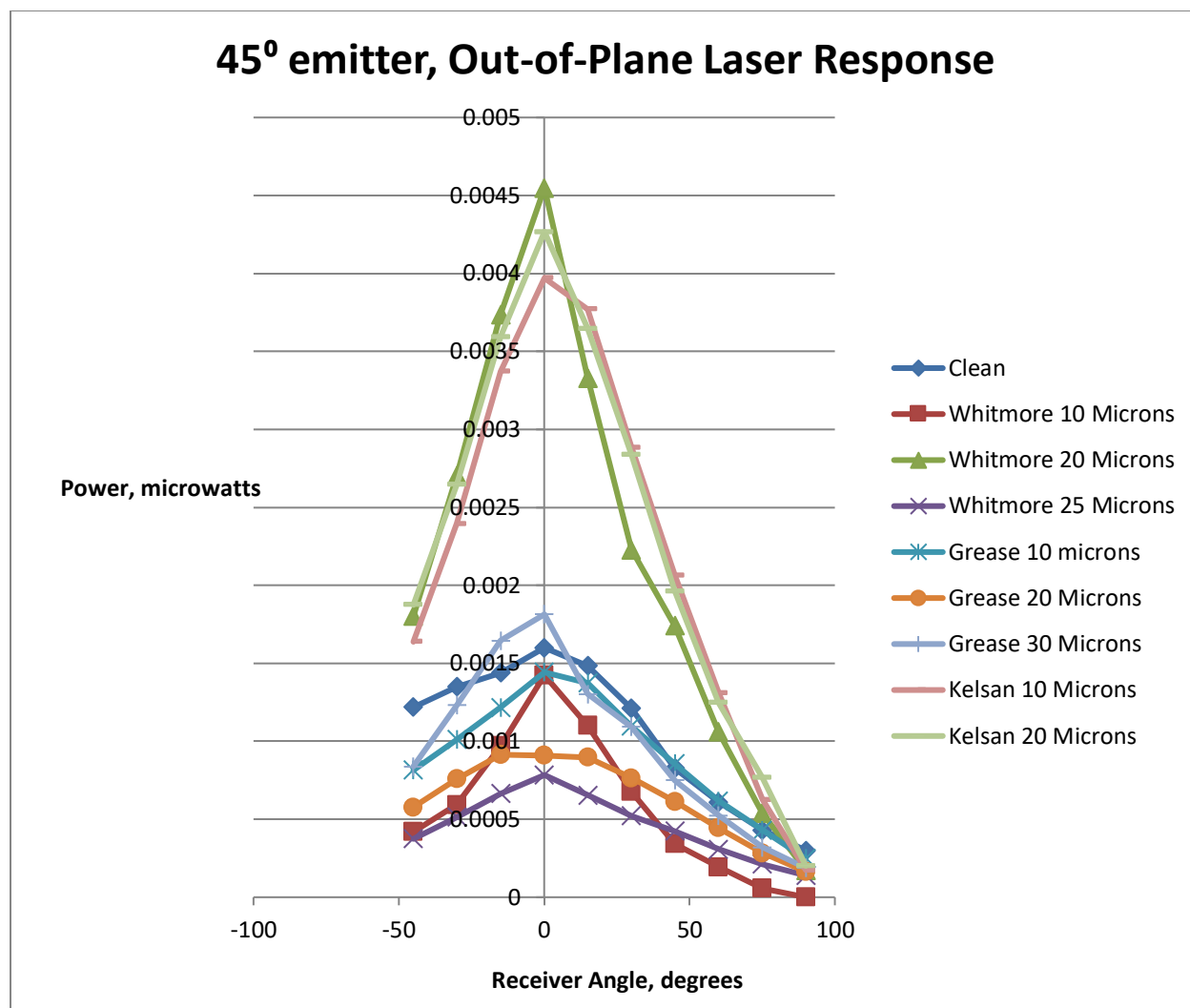


Figure 3-17: Out-of-plane testing for various top-of-rail materials and thicknesses for a fixed emitter at 45°. Thicknesses are based on shim application.

Between the two planes of responses, a 3D lobe could be interpolated using Matlab. A figure of this response can be seen below in Figure 3-18. All data was taken in microwatts and a log plot drawn from the raw data to accommodate for large specular responses.

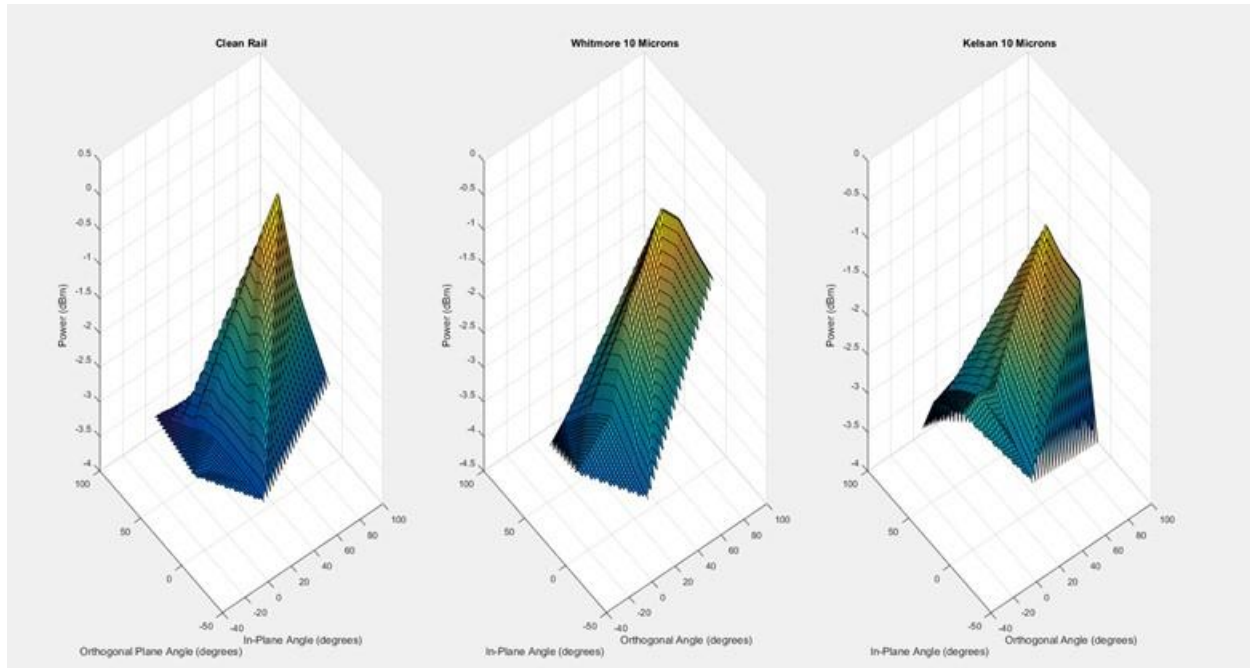


Figure 3-18: 3D interpolated response using Matlab. These are the responses for three top-of-rail conditions with a fixed emitter stimulus at 45° .

Graphs, both 3D and in a single plane, were examined to identify which configuration had the most distinguishing properties. This series of experiments shed light on several properties of the materials tested. As mentioned in chapter 2 of the literature review, contamination of a surface leads to decreased specular reflection and increased diffuse scattering. In most cases, the peak specular reading decreased as thickness increased. Additionally, in most cases, the response curve of the clean rail was sharper than that of the conditioned rails, speaking to the decrease in diffuse scattering. Another interesting point was the fact that oily substances such as flange grease enhanced the specular reflection, exceeding the maximum specular readings even for the clean rail. At this point, characteristic lobes of light were hoped to discriminate between various top-of-rail conditions. However, these ended up being too sensitive to consistently identify condition responses.

Instead, using the data drawn from this set of experiments, ratios were initially developed which compare diffuse scattering to specular reflection. These ratios were taken for every angle, and by definition the ratio at a given specular angle would be 1. This idea stemmed from the concept of Lambertian Scattering but does not directly employ Lambert's Law. These ratios were later further developed to include information about angle of stimulation and surface roughness. This will be discussed in Chapter 4. A table of these ratios can be seen in Table 3-4 for a laser stimulus at 45° . The table has been color coded to emphasize the angles which were imperative to the final prototype design. From this data, the ratio at the 60° angle categorized the type of top-of-rail material by sharing the approximate same order of magnitude; the ratio at the 0° angle from the vertical consistently increased with increasing thickness and can approximate the relative thickness of the material. While other angles accomplished this same phenomenon, practicality of construction and consistency with all tests were considered before making the final design

decisions. Additionally, these magnitudes required further calibration, as it will be explored later in chapter 4, but served as the foundation for the final design of the prototype.

Table 3-4: Table of the ratio of specular reflection to diffuse scattering at a determined angle. The table has been color coded to emphasize the ratios which were imperative to final design.

Ratio compared to Specular at 45 degrees									
Angle	Whitmore 10µm	Whitmore 20µm	Whitmore 25µm	Grease 10µm	Grease 20µm	Grease 30µm	Kelsan 10µm	Kelsan 20µm	Clean
-30	319.1366906	263.8173361	296.3176064	10393.02213	15025.71877	26024.52588	55.21483916	709.5176222	2135.808
-15	160.7246377	185.034467	250.745542	7269.176051	11218.87128	16632.64376	40.68652895	482.5072484	2574.211
0	5.85997358	83.0172346	154.8813954	5960.770356	6520.441729	9321.960314	25.27460717	262.4314786	2445.5
15	1.975066785	8.727558534	63.02585284	3477.448379	2341.066307	3418.430418	11.0165839	23.20584329	149.5719
30	0.486136986	2.288534548	2.232094485	138.7362511	73.87068438	147.168868	3.273020822	5.438530968	2.852061
45	1	1	1	1	1	1	1	1	1
60	4.411735455	2.682381061	1.476702509	168.8094971	93.0086805	153.8351315	3.935600482	9.389827776	27.94059
75	16.95394611	6.426439232	3.690433536	903.9551411	642.4288724	839.6475974	11.03623052	29.31633252	243.9401

3.5 Fluorescence Sensor Testing

Testing with the fluorescence sensor was also initiated at this time. The sensor used was the Balluff BLT 31M, the same sensor as used in the initial design. The UV emitter and corresponding detector are within one unit, but does not pose the same issue as the Keyence sensor with this same configuration. In this case the UV light supplied is not what the detector is sensing, but rather the UV light exists to excite the target so that it will fluoresce. When it fluoresces, visible light is emitted by the target, typically in the blue spectrum. This emitted light is detected by the sensor, rather than the reflected and scattered input light in the Keyence laser.

Studies prior to this revealed that the fluorescence signature of flange grease increases with increasing thickness while all other top-of-rail materials exhibited the inverse effect. In these studies, “dry” refers to a clean rail, and “thick,” “medium,” and “thin” are all relative terms of significantly higher thicknesses than that of the angle experiments which utilize thin shims. Additionally, the overall fluorescent signature of grease is much higher than that of other materials. Figure 3-19 shows the mean voltage at varying thicknesses for grease and other top-of-rail materials obtained from laboratory testing.

This property of flange grease was utilized to identify flange grease contamination on the top-of-rail. As other fluorescent signatures are low, increased readings can identify mixing of flange grease with top-of-rail directly. Table 3-5 shows former lab experimentation with this very concept. Figure 3-19 demonstrates the inverse effect of grease readings increasing while other materials decrease with increasing thickness. Additionally, experiments were carried out which varied the amount of mixing each top-of-rail material had with flange grease. In this case as well, increasing magnitudes with increasing mixing levels demonstrate the ability to identify flange grease from its fluorescent signature.

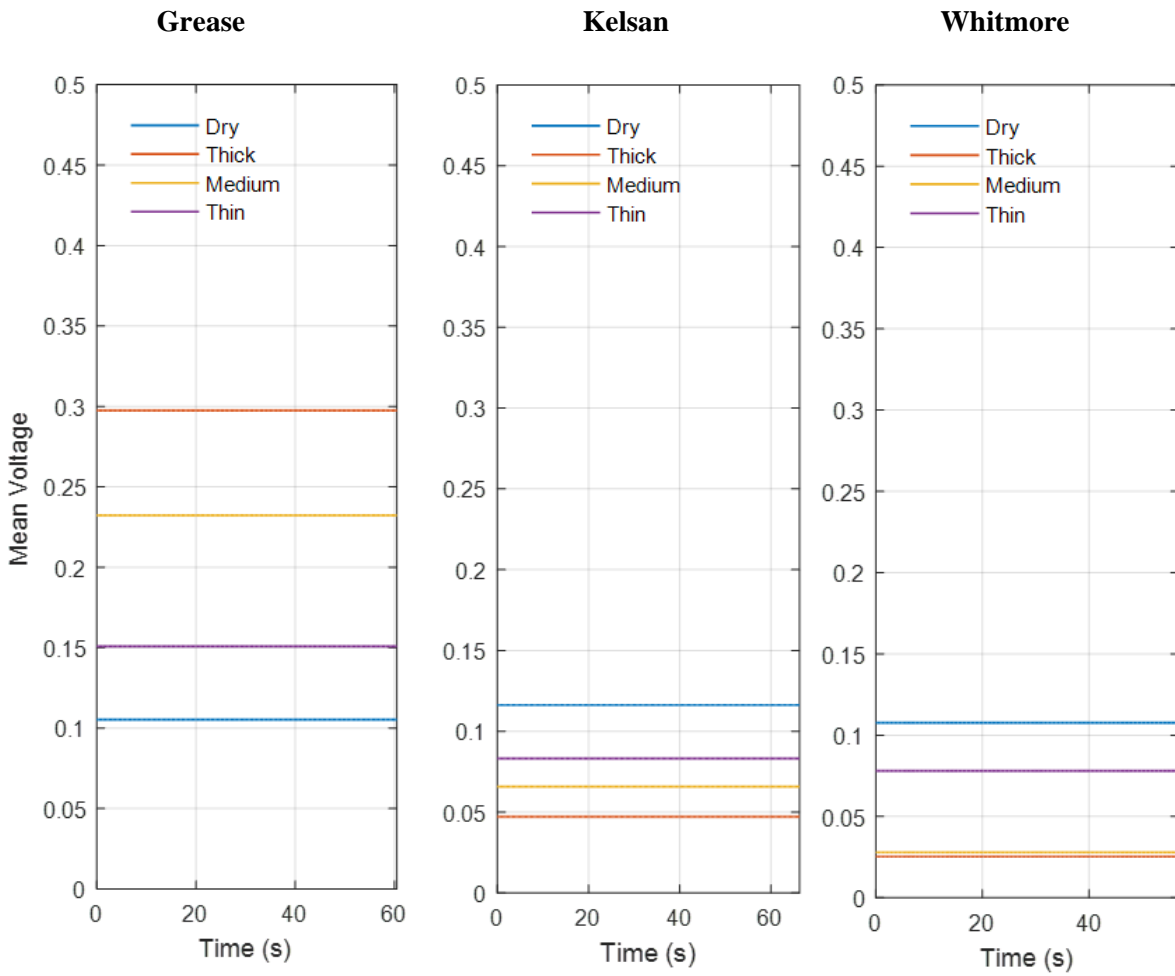


Figure 3-19: Comparison of average readings on Balluff fluorescence sensor as thickness varies for various top-of-rail friction modifiers and flange grease.

Table 3-5: Laboratory testing on mixing of flange grease with various top-of-rail materials

Mixed With	Kelsan	Whitmore	Loram
100% Grease	0.14	0.19	0.15
66% Grease	0.11	0.04	0.10
33% Grease	0.05	0.02	0.07
0% Grease	0.02	0.01	0.05

3.6 Summary of Design Aspects for Prototype

Following the parametric study and laboratory experiments, several design parameters were chosen for the prototype of the device for this study. All decisions were based on experimental testing with a background in optical theory to bolster the decision. Practicality of construction was considered, in addition to consideration of use in the industry by railway professionals.

First, the design decision about beam spot geometry was considered. As it was concluded from the experimentation, a focused beam was influenced too much by minor defects in the surface roughness while the collimated beam produced more consistent readings. The final design of the box includes a 635nm laser within a two element one-inch diameter expansion telescope which expands the beam to a diameter of 1cm. This allows for maximum visibility of the tapeline, on which top-of-rail material is directed considering the rail/wheel contact patch.

Next, the minor influence of sunlight affected readings which disrupts the already low signal-to-noise ratio and had to be eliminated. Therefore, the prototype was to be designed to exclude all external sunlight. All detectors must either be shielded from sunlight using optical filters or set within a case which eliminates all sunlight, or both. This guarantees consistency in readings despite shading from weather or environmental conditions.

The sensitivity to extremely small movements in the Keyence sensor required two aspects for full mitigation: relative movement between the rail and sensor must be eliminated, including vibration; the laser emitter and corresponding reflective detector should be separated to allow for more flexibility and predictability in readings. Moving to a stationary design can eliminate the major source of vibration and movement to alleviate the first aspect of this requirement. Separating the emitter and receiver will no longer couple displacements such that a slight change in angle would displace the emitter so that the scattering which was designed to be near specular is in fact quite far from specular. These two design changes will eliminate a large portion of ambiguity and avoid saturation.

Angles of the emitter and receiver were explored after laboratory experimentation specific to the industry. The profiles which were obtained through experimentation were considered characteristic of each top-of-rail condition, considering type and thickness of material. Each plot was examined for largest differences in curves to ensure largest differentiation between conditions. After considering this and the ratio of specular reflection to diffuse scattering at each angle, two angles were selected which displayed the most promise for ease of construction and discretion in

reading. Fixing the laser emitter at a 45° angle, the detector angles selected for with ratio consideration were at 0° and 60° from the vertical.

Finally, the lab experiments with the fluorescence sensor justified it as a tool for more sensing capability of this device. This sensor is utilized for its ability to identify the presence of flange grease due to its fluorescence signature and lack of signature for top-of-rail materials used in the industry. This sensor will remain in the design, fixed in the upright position directly normal to the rail surface. Though the detector and emitter are together in one unit, this sensor is appropriate because of the nature of detection.

3.7 Prototype Design and Capabilities

Considering all conclusions from section 3.6, the construction of the prototype included all design requirements and will be detailed in this section. This includes materials used and specifics on materials chosen and operating procedure. A diagram of the prototype can be seen in

Figure 3-20.

The basic design of the prototype is a wooden box outfitted with appropriate instrumentation for the detection of lubricity on top-of-rail. The box is stationary with a slot of 3 inches cut from either side, on which the device will sit atop a rail section. The outer dimensions of the box are 8"x20"x20". The outer casing is made of cabinet-grade wood, sealed with spar-varnish. It has a removable bottom face which protects the inner instrumentation from outside contaminants, which must be removed in order to be utilized. All instrumentation is fixed to the back side of the box, and has a support stand so that it can remain upright when atop a rail section.

A diode laser from Thor Labs of 635nm wavelength (red) and 3mW power was selected as the emitter. This emitter was fixed at a 45° angle to the rail. Three square silicon photodiode detectors were utilized to obtain the ratios mentioned in section 3.5 and 3.6. These were fixed at the specular reflection at 45° , and at 0° and 60° from the vertical. In order to fit into the dimensions of the box, first-surface aluminum mirrors were utilized to compact the orientation of the laser and detectors. These mirrors had a reflection rating of about 80-90%. All angles were calibrated to the surface line where the rail will rest. Each detector was fitted with a laser-grade interference filter at 635nm, with a 10nm full-width half-maximum bandwidth and 80% peak transmission. This ensures that the only light being detected is within a narrow band of 635nm, making it resistant to sunlight. The detectors were also fitted with lenses for a spot photometer configuration, allowing the beam spot on the rail to be reimaged to the detector instead of relying on scattering light and its solid angle. The Balluff 31M detector was installed near normal to the rail and within its specified height for detection according to its manual. It was later modified to be slightly rotated about 2° from normal to avoid reflection of the UV laser pump light being reflected back into the sensor, thus avoiding saturation, especially along banked rails.

The DATAQ instrument utilized in the parametric study was installed on the prototype as well. Trans-impedance amplifiers were utilized for each detector to avoid saturation, set at 10^5 on the specular channel and 10^6 on the 0° and 60° detectors. This moved the dynamic range of the laser sensor system to 1-10V. The Balluff 31M sensor was installed without any amplifier and remained with a 1-5V dynamic range. All sensors can be accessed through an external switch, and live readings can be taken from a dial and multi-meter installed externally to the box casing. The

DATAQ instrument is also installed externally to access the storage device and initiate data recording sequences. The device is powered by two rechargeable 12V lead-acid batteries.

The prototype is designed such that the laser and fluorescence detectors are looking at two different locations within a few inches of each other. The rail is assumed to be approximately the same between these two conditions in a practical sense. It can be used for single point detection along the length of the rail. It is under 20lbs and can be carried and transported with ease. This instrument was constructed and additional lab testing took place to calibrate the device, and was later taken to the field for field testing and validation.

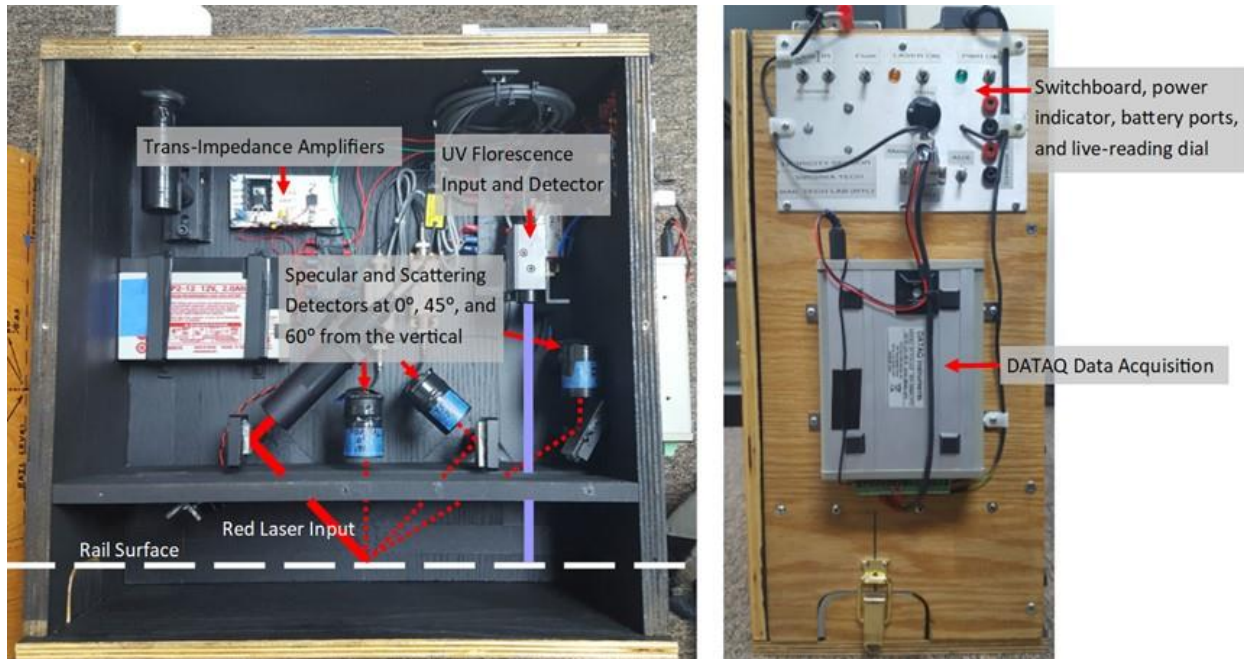


Figure 3-20: Prototype design, internal structure and user interface.

4. Laboratory Evaluation of Prototype Unit

This chapter will explore the laboratory testing which was performed upon the completion of the prototype. The device was in need of calibration and validation against previous measurements. This was in preparation for field testing and validation to industry practice. According to the experiments and analysis in this chapter, the device is operational and successful in determining top-of-rail conditions in a binary manner.

4.1 Operation Procedure

This section will briefly outline the switch schedule and basic operation of the prototype. Assuming the rail is already conditioned to the appropriate testing environment, the device, when charged, is ready to record data when loaded with an SD card in accordance with the DATAQ instrument.

Figure 4-1 outlines the switches on the switchboard. The master switch is turned on, which gives power to the DATAQ system and the rest of the device. There are two separate switches which turn on the two sensors of interest in this research: the laser and the fluorescence sensor. Live readings can be taken by hand by engaging the dial to the appropriate position and reading the multi-meter atop the prototype, as seen in

Figure 4-1.



Figure 4-1: Diagram of box switchboard (left) and controls (right).

In order to conduct a test on the same patch of rail, the device is placed on top of the rail and the stability rod is engaged. The angle of the rail cant is determined and matched to the box placement using an external digital level. Once aligned, the master switch is engaged to turn on power to the unit. The laser reading is taken first, accomplished by engaging the laser switch and recording data by pressing and holding the main button on the DATAQ system itself, which is installed externally to the prototype casing. The button is pressed and held again a few seconds later to stop recording. In order to get the fluorescent reading at the same location, the unit must be moved forward 5 1/8" and leveled. Taking the fluorescent readings involves disengaging the laser switch and engaging the fluorescence sensor switch, and repeating the sequence on the DATAQ instrument to record. At this point, both measurements of interest have been recorded and stored. Live readings can also be taken at each position for personal records.

4.2 Prototype Calibration

In order to use the prototype against the data already collected from laboratory experiments, a calibration factor had to be developed which considered the equipment installed within the prototype. This calibration factor considers the efficiencies of all components through which the laser beam will pass or on which the beam will be reflected. This calibration factor has been compared against Lambertian Scattering Theory and is validated. These calibration factors will be used for all data collected by this prototype.

Within the prototype, there are three laser detectors at various locations, as seen previously in

Figure 3-20. A table of the constants which define the efficiency of various components, as well as the laser output power can be seen below in Table 4-1.

Table 4-1: Table of prototype component constants

	Normal Scattering Detector	Specular Detector	60° Scattering Detector
Laser Output	$1.30 \times 10^{-3} \text{ W}$	$1.30 \times 10^{-3} \text{ W}$	$1.30 \times 10^{-3} \text{ W}$
Expansion Telescope Transmission	0.96	0.96	0.96
Surface Reflectivity (steel)	0.75	0.75	0.75
Mirror Reflectivity	1	0.80	0.80
Filter Transmission	0.75	0.75	0.75
Lens Transmission	0.98	0.98	0.98
Detector Responsivity	0.7	0.7	0.7
Electronic Gain	1.00×10^6	1.00×10^5	1.00×10^6

Considering all of these factors, the expected output for the specular case would be the multiplication of all of components listed. This estimation does not include the solid angle because

of the nature of the detectors. Within the prototype are spot photometers, which effectively reimages the target from the rail to the detector. This estimation of expected power was compared to actual lab results which consider scattering. A simple way to consider scattering is to normalize two detectors against the other one. Assuming Lambertian Scattering, where the intensity of reflected light is constant over a polar angle, we can take the readings from an assumed perfect Lambertian Scattering surface and normalize the specular and sixty degree readings to the scattering reading normal to the surface. Table 4-2 shows the values of the prototype against a white card, acting as a perfect Lambertian scattering surface.

Table 4-2: Relevant raw data and calculated scattering factor for prototype calibration.

	Normal Scattering Detector	Specular Detector	60° Scattering Detector
Raw Data, Steel	0.6490	0.9350	1.5070
Raw Data, White Card (V)	2.8190	0.0665	0.4500
White Card Scattering Factor	1.0000	42.3910	6.2644

Multiplying this White Card Scattering Factor to the original raw data for the steel validates the calibration method in the specular component. Table 4-3 shows the compared values in the specular detector.

Table 4-3: Actual and calculated calibration factors, including error.

Expected Value using Transmission Constants	38.53
Actual Data from Lambertian Scattering Factor	39.64
Error	2.88%

Using this calculation method, the calibration constants used in all experimentation with this prototype can be seen in Table 4-4 below:

Table 4-4: Final calibration constants for prototype.

Normal Scattering Detector	Specular Detector	60° Scattering Detector
1	39.6	6.63

4.3 Empirical Model for Determining Lubricity

After the calibration was complete for accuracy and reliability in the sensor readings, a method needed to be determined to distinguish if any sample of rail was adequately conditioned using traditional top-of-rail friction modifiers used by the industry today. In order to achieve this,

responses were considered which determined the design of the prototype, as well as the influence of the surface roughness.

The initial ratio which was developed determining the “type” and “thickness” which was mentioned in chapter 3 was modified empirically to work better in a numerical environment. Several calculations were considered which scaled the orders of magnitude for “type” and “thickness” in this ratio, and the calculation which provided the most consistency was the natural log of the ratio. In this way, equations 2 and 3 were determined, as seen below:

$$SMC = \ln\left(\frac{P_{45^\circ}}{P_{60^\circ}}\right) \quad 2$$

$$SMT = \ln\left(\frac{P_{45^\circ}}{P_{0^\circ}}\right) \quad 3$$

In these equations, SMC refers to “Scaled Material Category” and SMT refers to “Scaled Material Thickness,” where P_{45° is the output for the detector at the 45° specular orientation, and P_{60° and P_{0° are the outputs for the detectors at the scattered 60° and normal orientation. These are two separate metrics which determine the overall level of lubricity on top-of-rail conditions. It should be noted that the Scaled Material Thickness (SMT) calculation does not directly relate to a physical thickness in a measurable way yet, and is only used in a relative sense, and more importantly, as a second dimension to qualifying rail condition.

The surface roughness of any particular sample had to be considered in order to provide consistency in readings between rail samples. Initial experimentation showed that there was consistency in ability to determine top-of-rail conditions for one sample, but those same quantities were shifted when tested on a different rail sample. Table 4-5 demonstrates this phenomenon through the changes in standard deviation between rail samples versus the entire set of data. It should be noted that a change in 0.5 was significant in that it shifts the readings to another range of conditions. The only explanation for this phenomenon was that the influence of surface roughness is significant.

Table 4-5: Raw data on various rail samples with standard deviation.

Rail Sample	1 shim thick	2 shims thick	3 shims thick	Average	Standard Deviation
1	2.508575	2.795846	2.575425	2.626615	0.150321
2	1.733357	1.734653	1.575513	1.681174	0.091508
3	2.273691	2.564408	2.470488	2.436196	0.148361
Standard Deviation of all samples:				0.448071	

Reviewing the literature of calculating surface roughness allowed an empirically derived formula to be used for this research. As mentioned in chapter 2, the most fitting determination of surface roughness for this application is the geometric calculation using the root-mean-square (RMS) which can quantify in a non-dimensional coefficient which can be used in our calculations. Though there are many ways which have been published to determine the roughness of a surface

using the root-mean-square, Theodore Vorburger's equation for smooth surfaces was used in part for calibration [16]. It takes from theory of total-integrated-scatter and defines surface roughness as follows:

$$Rq = \left(\frac{\lambda}{4\pi \cos \theta_i} \right) \left(\ln \left(\frac{P_0}{P_{spec}} \right) \right)^{0.5} \quad 4$$

This equation demonstrates the relationship between the RMS roughness Rq and specular and scattered light. This equation was modified for this research for scaling purposes and to meet the design limitations of the prototype. As there are only three detectors for the emitted laser beam, total scattering is not able to be determined. Therefore, scattering was only considered from one detector, particularly the detector in the 60° orientation. Additionally, the factor of the wavelength was eliminated as it scaled the calculation far below its influence. However, the angle was considered, especially as Lambertian Scattering was used for the initial calibration of the instrument. Therefore, the metric which was empirically used for this research has been coined the Surface Roughness Coefficient (SRC) and is calculated as follows:

$$SRC = \frac{1}{\cos \theta} \left(\frac{P_\theta}{P_{spec}} \right)^{0.5} \quad 5$$

In this equation, θ represents the angle of the detector in the scattering orientation. For this application, the 60° detector is used so θ is 60, and P_θ is its output; P_{spec} is the output of the detector in the specular orientation. Values for this quantity adequately demonstrate the influence of surface roughness on readings.

From these calculations, two metrics have been determined which can quantify lubricity conditions, seen in equations 6 and 7.

$$TRM = SMC * SRC \quad 6$$

$$TRT = SMT * SRC \quad 7$$

Here, TRM refers to the Top of Rail Material, while TRT refers to the Top of Rail Thickness. Again, these do not relate to physical thicknesses but merely a metric which has a positive correlation with thickness of top-of-rail material. When these calculations are applied to the data collected previously, a graph can be formed which demonstrates the differences in conditions. In a practical sense, multiple top-of-rail materials will not be on a single rail, as wayside lubricators are filled with one known and determined material which carries down a distance along the rail. For this reason, the following graphs in

Figure 4-2 and

Figure 4-3 compare one friction modifier to clean rail conditions, and do not compare to each other.

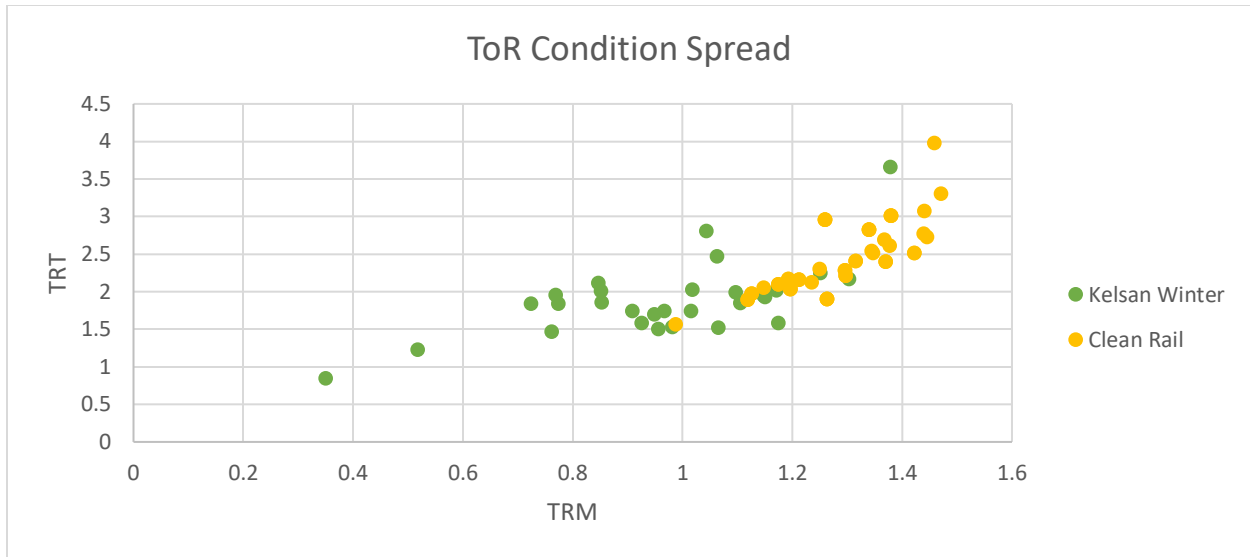


Figure 4-2: Kelsan and clean rail test data

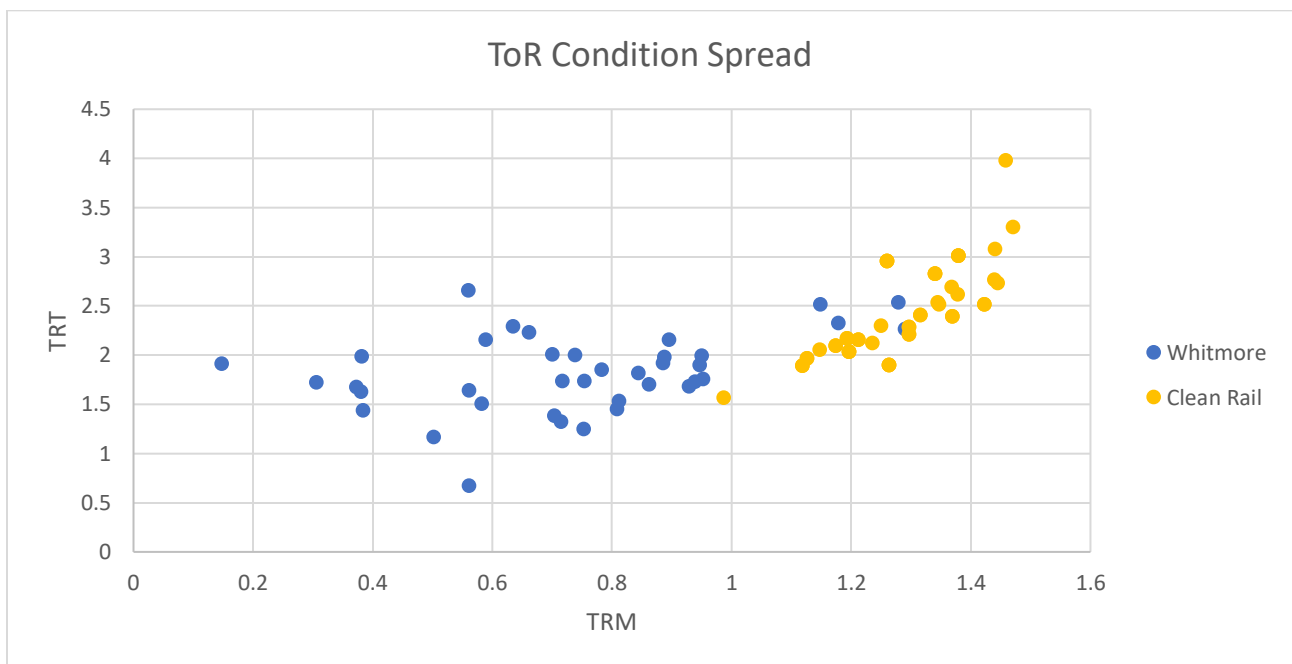


Figure 4-3: Whitmore and clean rail test data

Clear clusters are shown in either case, making linear discriminant analysis an ideal statistical tool to determine if a particular rail sample has adequate friction modifier present on top-of-rail. When comparing Kelsan Winter to a clean rail, linear discriminant analysis predicts the correct condition 81.4% of the time, while the comparison of Whitmore to a clean rail predicts the correct condition 92.4% of the time.

4.4 Prototype Experiments with Fluorescence

The prototype was also used to re-examine the grease-mixing phenomenon which was mentioned in chapter 3. Previously, mixing grease with common industry top-of-rail materials was evaluated for relatively thick layers. What was demonstrated was an increase in fluorescence with increasing presence of grease, as grease has been identified as a fluorescent material under ultraviolet light while other top-of-rail materials are not and have very little fluorescent signature. The same grease mixture concentration was upheld as in Chapter 3 but applied in very thin layers by applying the substance and rubbing it off using a black, non-fluorescent cloth. Four points on a rail were examined in a laboratory setting. The behavior in this run of tests was similar but had some abnormality due to the thin nature of the material.

Four locations were marked and conditioned prior to testing. This included the full cleaning process of rubbing alcohol, hydrogen peroxide, and distilled and deionized water. Each location was conditioned with a mixture of 33%, 50%, and 66% grease mixing. Two industry products, Kelsan and Whitmore, were examined in this set of experiments.

Figure 4-4 and Figure 4-5 demonstrate the results of these experiments at extremely thin layers. Between the four points, the Whitmore top-of-rail material responded more consistently by responding with small increases in response with increasing flange grease presence 91.7% of the time while the Kelsan mixing only held this behavior in 81.8% of its comparisons.

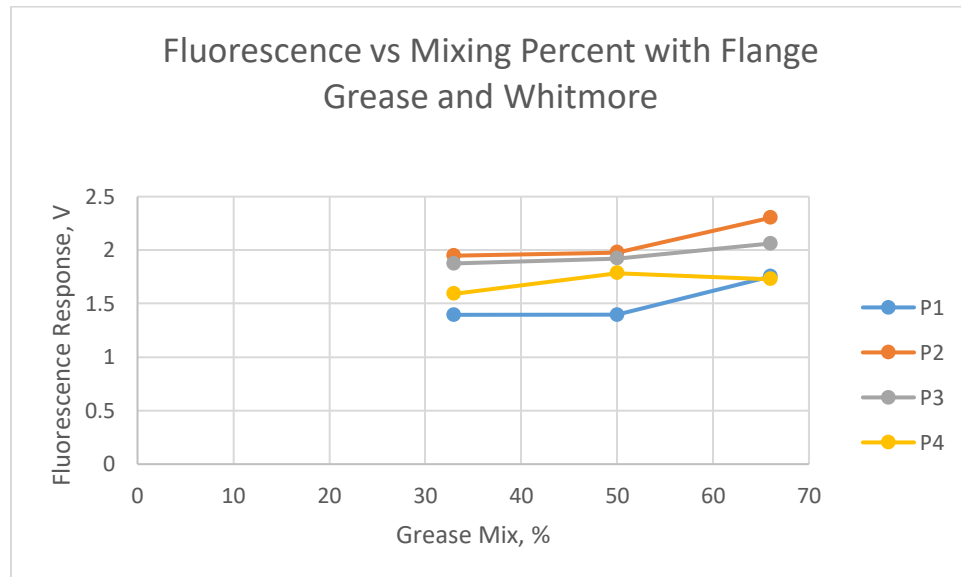


Figure 4-4: Response of Balluff fluorescence sensor to increasing grease mix with Whitmore top-of-rail material.

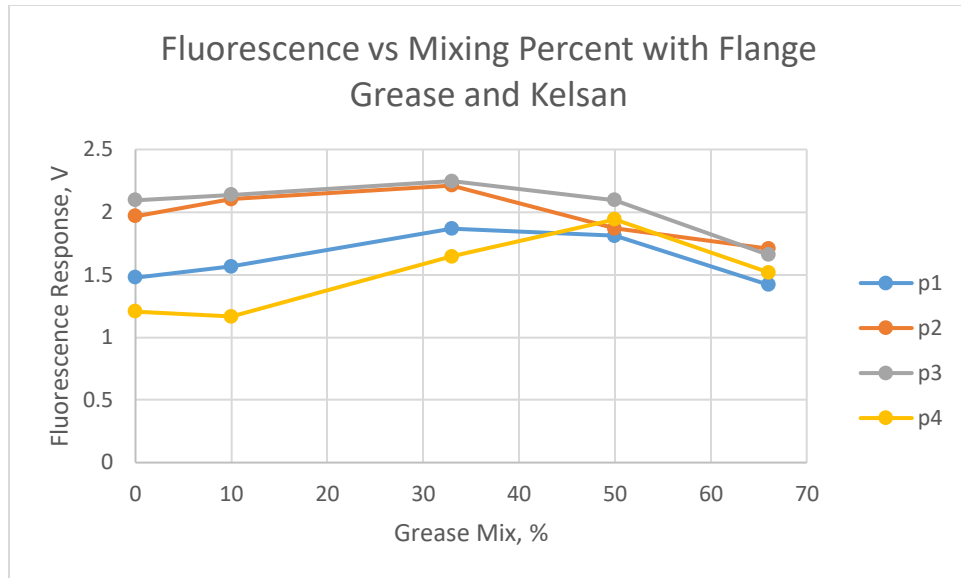


Figure 4-5: Response of Balluff fluorescence sensor to increasing grease mix with Kelsan top-of-rail material.

This was explored further in additional testing, looking at the macro appearance of a top-of-rail friction modifier with 33% grease mixing not considering thickness numerically, but at thicknesses larger than that of the previous experiment. Figure 4-6 and Figure 4-7 show consistent increase in readings between the two plain friction modifier material and the presence of grease. This suggests that this response is more consistent with thicker material content on top-of-rail.

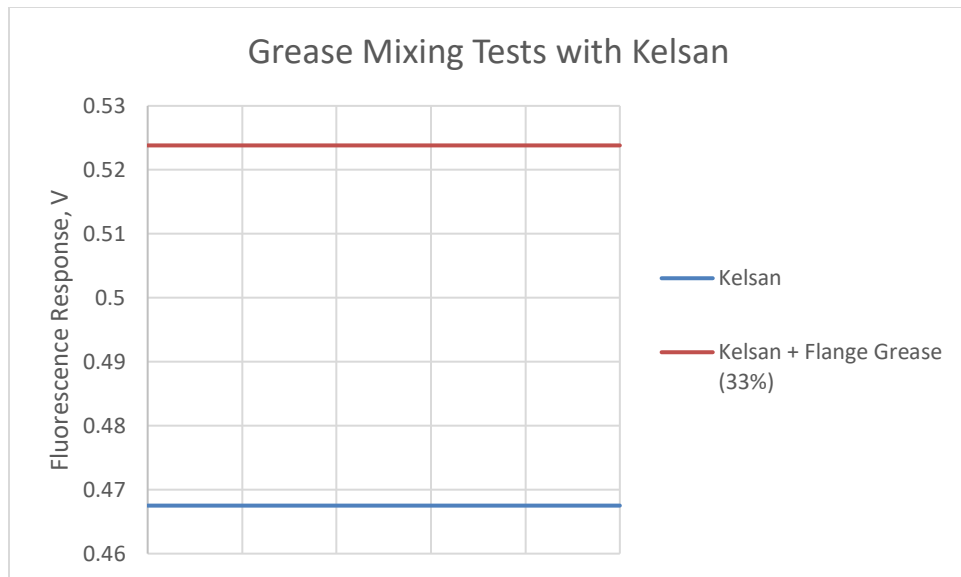


Figure 4-6: Additional testing of the fluorescent response of Kelsan top-of-rail friction modifier and flange grease (33%).

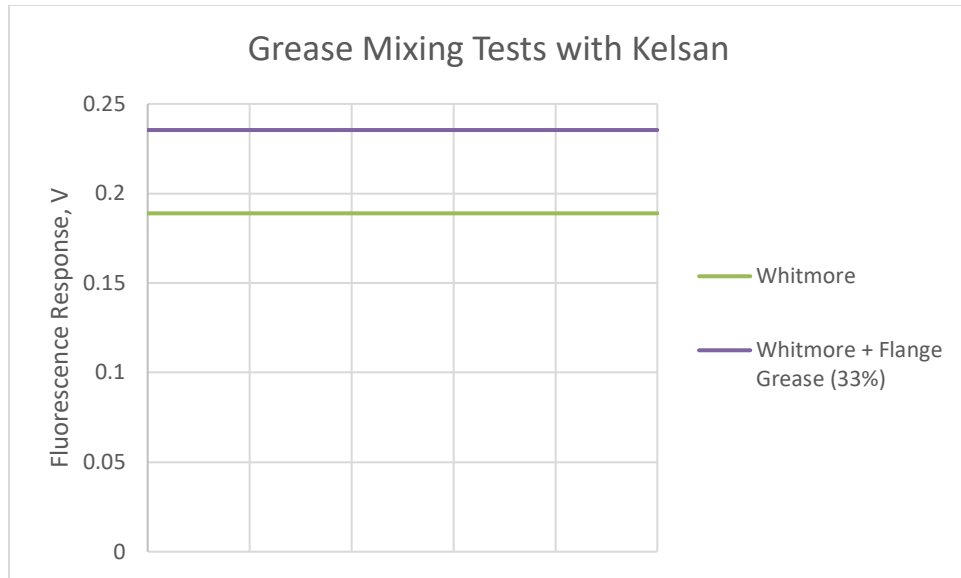


Figure 4-7: Additional testing of the fluorescent response of Whitmore top-of-rail friction modifier and flange grease (33%)

5. Field Testing with Prototype

This chapter will outline the field testing which took place to validate the prototype design. It will first review the testing procedure, including location descriptions and expected results. It will review the expected results as they relate to the predictions from patterns outlined in previous chapters. Finally, it will conclude implications of this field test, justifying the success of this field test in validating the design of this prototype.

5.1 Testing Logistics

On August 3rd, 2016, Norfolk Southern hosted the Railway Technologies Lab in testing the lubricity prototype. Testing took place along one stretch of rail at three different points in Ironto, VA, just off of mile marker 128 on Route 460. These points are outlined in Figure 5-1.

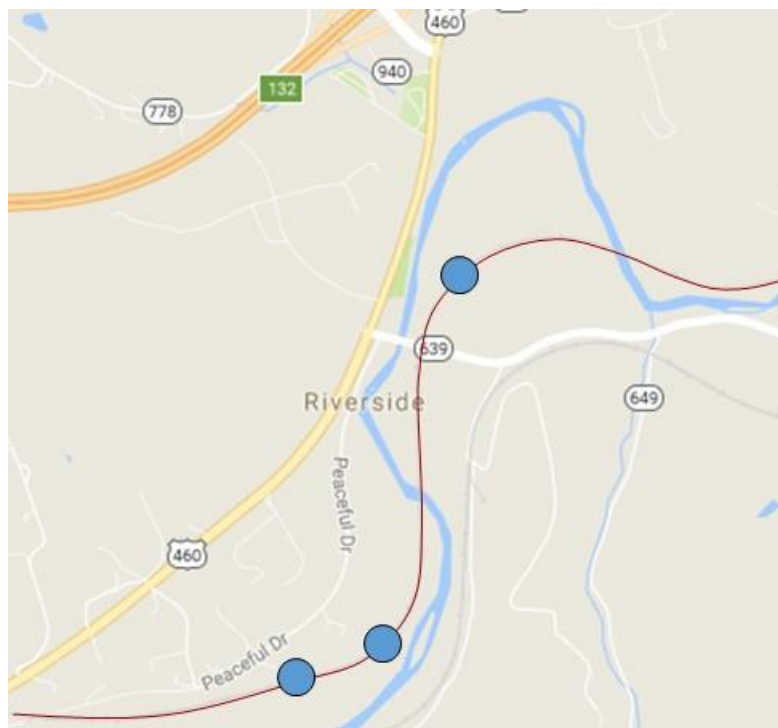


Figure 5-1: Map of three locations along Norfolk Southern Rail for field testing in Ironto, VA.
Picture from maps.google.com.

For time purposes, these points were selected at three locations with different lubricity conditions. The first testing location was at the site of the wayside top-of-rail lubricator, but before a flange grease lubricator for east-west traffic. The second location was a quarter mile westward of the first point, where lubrication conditions were adequate in accordance to product specifications for carrying distances. The third location was 1.07 miles westward from the lubricator, and was a location which was indicated by Norfolk Southern professionals to be of questionable lubricity condition. At each of these three points, eight data points were collected by the prototype, four on either rail, two feet apart from each other. This was done for relative statistical certainty. The prototype was shifted such that the laser and luminescence sensor observed the same exact

condition. At one of the eight points in each testing location, the rail was cleaned so that a clean rail comparison could be made. Data was recorded using the DATAQ system installed on the prototype, by hand using the multi-meter live reading capability of the prototype, and all testing procedures were recorded via GoPro footage attached to the helmet of one of the graduate research assistants present for this field testing. Substantial photos were taken as well to document all actions and conditions present for field testing. Location was recorded at each of the three sites using GPS coordinates.

A schematic diagram can be seen in Figure 5-2 demonstrating the relative location of testing locations to wayside lubricators. It is important to note that according to the Norfolk Southern professionals, most traffic is westbound, or left to right in the figure. Testing locations are highlighted in red, including both rails. Testing at the first location was a tangent track; at the second location a left curve; at the third location, a right curve, which is not demonstrated in the schematic diagram.



Figure 5-2: Schematic diagram of testing sites (1, 2 and 3), including wayside lubricators. Most traffic is westbound, in this diagram: left to right.

The testing procedure for each site was as follows: the GoPro was turned on to record all actions for each testing site; four locations were measured and marked by masking tape, two feet apart, on either rail; the prototype was leveled to the ground and the proper switch sequence took place to obtain the laser response and was recorded; the prototype was toggled laterally along the rail to find a maximum laser output to accommodate for banking and recorded; the prototype was shifted for the fluorescent sensor and leveled to the ground, and the proper switch sequence took place to obtain the fluorescent response; the data acquisition process was repeated for the remaining seven locations; pictures of each of the eight testing locations per site were taken, as well as pictures of the surrounding environment; a contact measurement was taken using the depth micrometer fashioned in the CVeSS lab by Dr. Andrew Peterson; the rail was properly cleaned at the first location; laser and fluorescence readings were taken on the single testing location.

5.2 Expectations of Field Testing

The test data graphed in chapter 4 is used to determine if a tested spot has adequate top-of-rail material. Two of the three sites tested had inferred levels of lubricity as adequate: the site at the Top-of-Rail applicator, and the site a quarter mile from the applicator. Product specifications range from 1-4 miles depending on the material (whitmore and kelsan product manuals). According to the product specifications of the material applied in the field, the curve 1.07 miles from the applicator should have had adequate top-of-rail material [20, 21]. However, the determination of the third site was on the basis of having questionable lubricity conditions according to Norfolk Southern professionals. Therefore, it was hypothesized that sites 1 and 2 would have adequate top-of-rail material, while site 3 would fall on the “clean rail” spectrum.

The fluorescent sensor was expected to respond according to the predicted response of the flange grease contamination. Because the first site was before the flange grease applicator for most traffic, it was expected to have very low levels of response. The second site was predicted to have the highest readings, as it is closest to the flange grease applicator for most traffic. As the third site was predicted to have minimal top-of-rail material, it was also predicted to have minimal flange grease contamination.

5.3 Test Results

This section will outline the conclusions from the field test after data analysis. The design of this prototype for field applications will be justified against the lab data from known conditions. Other evidence will be presented which could potentially serve for further study of top-of-rail material with the rail and wheel.

5.3.1 Laser Sensor Results

Each point of field data was compared to the test data set gathered from laboratory experimentation, as this was the basis for linear discriminant analysis to determine if a point has adequate top-of-rail material. As clean rail was taken at only one location per site, this data was used to determine the Surface Roughness Coefficient which was assumed to be the same for all eight data points. This seemed to be an adequate assumption, as the standard deviation of raw data values per site is very low. A table of these values can be seen in Table 5-1. It should be noted that there is a higher standard deviation at the first field testing site. This is believed to be due to the fact that the physical appearance of the rail was very different along the eight points, as this was the site of direct top-of-rail material distribution. Clumps of top-of-rail friction modifier therefore remained present and led to a high variance of physical appearance and therefore a high variance in optical response. It should also be noted that the following numbers and analysis are for the toggled maximum value, as this approximately considers the banking along the curves and is more accurate as a result.

Table 5-1: Table of raw, unprocessed and uncalibrated data of three laser sensors during field testing in Ironto

		Normal Sensor	Specular Sensor	Sixty Degree Sensor
Site 1	East	0.16506	0.435848	0.306931
		0.146243	1.316153	0.270282
		0.238034	0.904001	0.283076
		0.114897	0.15978	0.195029
	St.Dev	0.052255	0.51082	0.048316
	West	0.10181	2.148944	0.14383
		0.062755	2.891046	0.108217
		0.11827	0.903679	0.158214
		0.049863	0.242078	0.082458
	St.Dev	0.032175	1.195195	0.034332
Site 2	Lo Rail	0.036072	3.759629	0.124599
		0.05479	3.030401	0.148987
		0.036891	3.89685	0.115015
		0.034232	3.196148	0.106746
	St.Dev	0.009594	0.422029	0.018285
	Hy Rail	0.086268	1.136566	0.144442
		0.083604	1.375717	0.151993
		0.103677	1.644065	0.166974
		0.115402	1.645941	0.172146
	St.Dev	0.015029	0.244821	0.012876
Site 3	Hy Rail	0.148326	0.243263	0.347544
		0.140781	0.233852	0.301418
		0.134394	0.247511	0.319856
		0.135749	0.245251	0.337613
	St.Dev	0.006306	0.006001	0.020327
	Lo Rail	0.036292	0.050232	0.100504
		0.04753	0.353814	0.181525
		0.052377	0.573542	0.140518
	St.Dev	0.008251	0.262773	0.040512

Each of these points were processed through the calculations described in chapter 4. These calculations were then put into graphical form against the test data collected in laboratory testing. These results can be seen in

Figure 5-3. It should be noted that the lab data included is that of a clean, untreated rail, and of Whitmore top-of-rail friction modifier as this was the material used on this portion of the track, according to Norfolk Southern professionals.

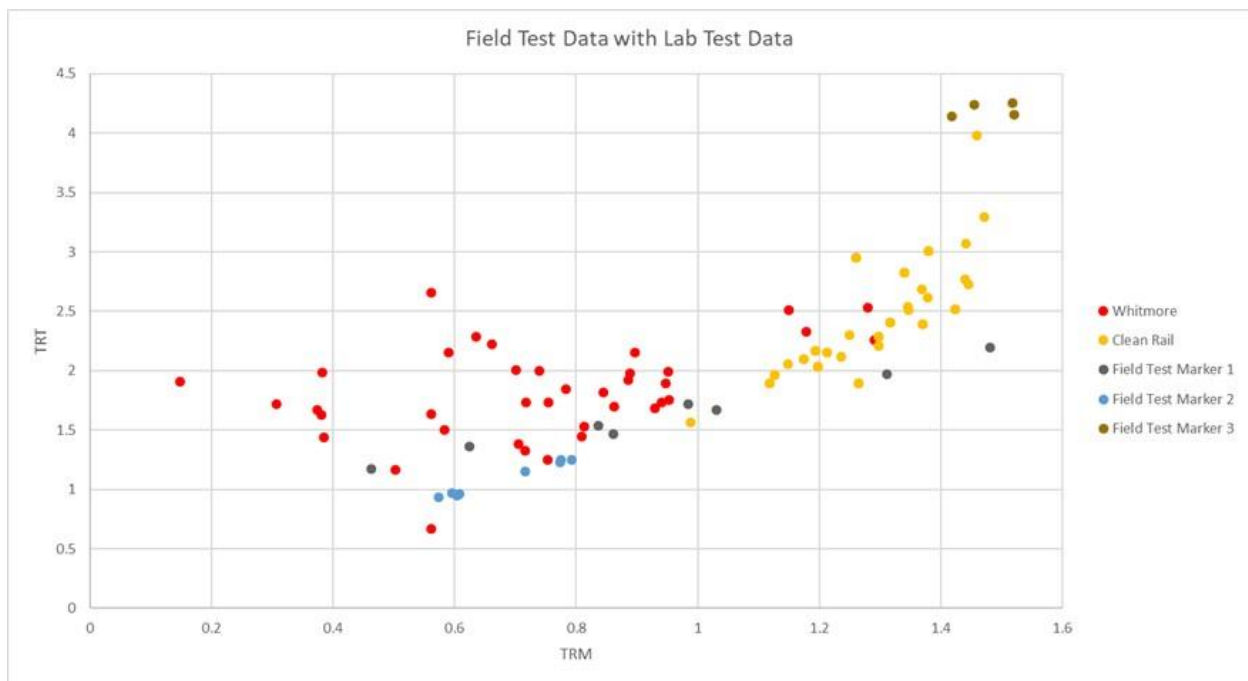


Figure 5-3: Field test data overlaid the lab test data for a clean rail and Whitmore top-of-rail friction modifier

Looking at the first site, labeled as “Marker 1,” there is a large spread. The explanation for this is mentioned above regarding the high variance in physical appearance of the rail. All testing done in the lab did not treat for these conditions, and therefore are not adequately represented on the test data. However, it should also be noted that in a practical sense, this prototype would not be used at a site such as this, as this device is intended to answer the question of whether a rail is adequately treated with top-of-rail friction modifier; at the site of top-or-rail material application, that question is already answered. That being said, knowing this area is adequately treated, the Linear Discriminant Analysis used on the test data is 75% accurate. A table of the probability of the classification between the two conditions—Whitmore on top-of rail and clean, untreated rail—can be seen in Table 5-2.

Table 5-2: Table of probability values of classification for the first site of field testing.

Table of Linear Discriminant Analysis on Field Data: Site 1		
Point Number	Classification	Probability
1		
	Clean Rail	0.007
	Whitmore	0.993
2		
	Clean Rail	0.343
	Whitmore	0.657
3		
	Clean Rail	0.097
	Whitmore	0.903
4		
	Clean Rail	0.001
	Whitmore	0.999
5		
	Clean Rail	0.963
	Whitmore	0.037
6		
	Clean Rail	0.995
	Whitmore	0.005
7		
	Clean Rail	0.463
	Whitmore	0.537
8		
	Clean Rail	0.078
	Whitmore	0.922

When analyzing the data at the second site, the numbers are much more clustered and consistent. Additionally, all eight points indicate that this portion of the rail is adequately conditioned with Whitmore top-of-rail friction modifier. The Linear Discriminate Analysis model predicted all eight points to be properly conditioned, ranging from 95.9-99.6% probability. Furthermore, this is congruent with the hypothesis at this location. A table of probabilities for this site can be seen in Table 5-3.

Table 5-3: Table of probability values of classification for the second site of field testing.

Table of Linear Discriminant Analysis on Field Data: Site 2		
Point Number	Classification	Probability
1		
	Clean Rail	0.034
	Whitmore	0.966
2		
	Clean Rail	0.017
	Whitmore	0.983
3		
	Clean Rail	0.041
	Whitmore	0.959
4		
	Clean Rail	0.033
	Whitmore	0.967
5		
	Clean Rail	0.003
	Whitmore	0.997
6		
	Clean Rail	0.004
	Whitmore	0.996
7		
	Clean Rail	0.004
	Whitmore	0.996
8		
	Clean Rail	0.004
	Whitmore	0.996

Finally, the data at the third site can be analyzed. First, it should be noted that the rail at this location showed visible signs of wear on its profile, as the prototype had difficulty fitting along the warped lo rail. For this reason, the data taken on the lo rail is not being considered. Considering the four points of data taken on the hi-rail, the Linear Discriminant Analysis classifies all four points as clean and unconditioned rail, ranging from 99.7-99.9% probability. This is also congruent with the hypothesis of this research. A table of probabilities at this site can be found in Table 5-4. The deformation of the rail is further justification that the rail was unconditioned.

Table 5-4: Table of probability values of classification for the third site of field testing

Table of Linear Discriminant Analysis on Field Data: Site 3		
Point Number	Classification	Probability
1		
	Clean Rail	0.997
	Whitmore	0.003
2		
	Clean Rail	0.999
	Whitmore	0.001
3		
	Clean Rail	0.999
	Whitmore	0.001
4		
	Clean Rail	0.998
	Whitmore	0.002

All points observed and covered in this section accurately depicted the condition of the rail from common sense and Norfolk Southern professional recommendation. For this reason, this serves as verification for the laser detector design of the prototype, thus answering the objectives of this project.

5.3.2 Fluorescent Sensor Results

The behavior of the fluorescent sensor was also consistent with all predictions made before the time of the field test. Site one was very low in reading, site two was the highest, while site three had bottomed out readings as observed in Figure 5-4. It is important to recall that even Whitmore and other top-of-rail materials had a slight fluorescent signature. The observation of no reading at the third location is therefore a further validation that there was no top-of-rail friction modifier present on the rail.

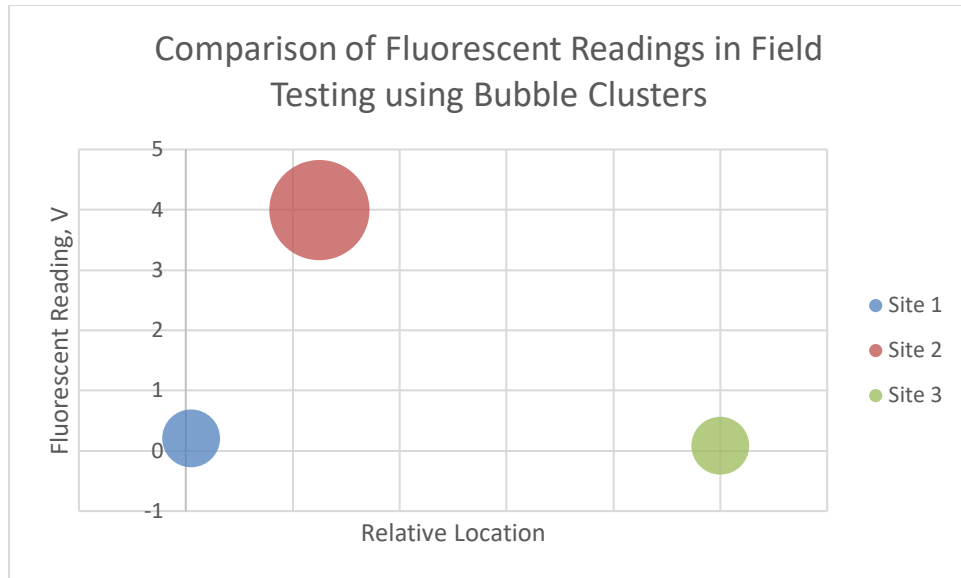


Figure 5-4: Clustered diagram of fluorescent response during field testing.

Though this data was consistent in predicted behavior, the magnitude of response was unpredicted at the second location. Most lab data taken for these friction modifiers and flange grease materials had a response of no more than 2 volts. However, at this site, the sensor saturated at much higher quantities than expected. This was analyzed to be the result of the banking at that curve. When the fluorescent data was taken, the prototype was level to the ground, using a simple bubble level. This method did not consider the banking angle and therefore the sensor was offset significantly than laboratory conditions. This sensor responded similarly to the initial Keyence laser sensor which saturated at certain angles directly reflecting input back into the sensor. Sites two and three were on a bank and therefore have unreliably inflated values. This is especially true for the hi-rail readings in the third site, where the prototype did not fit properly on the rail and sunlight was able to breach the opening while the red laser input became misaligned.

Despite these errors, the ability to detect flange grease contamination on top-of-rail is plausible through the use of a fluorescent optical sensor.

6. Conclusions and Recommendations

This chapter will discuss the findings of this research, including its implications on the industry today, and also provide recommendations for further development of this technology.

6.1 Summary

This research explored the feasibility of using various optical sensors for the detection of thin layers on a rail surface to benefit the rail industry in their rail lubricity application. Initial prototype construction and testing proved the detection of layers in a relative sense, and made clear the need for repeatable readings on an absolute scale. A parametric study took place afterwards which examined the best sensor configurations for such a device. A second prototype was configured and tested, both in a laboratory setting and in the field. Through an empirical analysis with aid from optical theory, a method of calculation was devised which can determine rail lubricity repeatedly and with statistical certainty. This method employed linear discriminant analysis of known conditions and the model proved to be 81.4%-92.4% accurate for industry materials in the lab, and 90% accurate in field testing. The consistency between lab and field tests and repeatability of the prototype design validates the legitimacy of this instrument as a means of determining rail lubricity.

6.2 Significant Findings

No published literature to date has determined an optical method of rail lubricity detection; this research is at the beginning of this application of lasers and optics in the rail industry for lubricity purposes. Some research has been performed on the detection of both thin layers and small defects in surface roughness, but no studies have tied these together on a shiny surface in a repeatable and significant way. As the rail industry invests significantly maintenance-of-way operations, preventing excessive wear and optimizing lubrication and friction modifier application is imperative. To do that, an understanding of the interaction of these materials on the rail and their properties needs to be developed. This research examined this interaction and allows a true measure to be taken against product specifications to determine its effectiveness in carrying down track. Additionally, optical devices can detect the contamination of top-of-rail with flange grease, as this is undesirable in practice.

Additionally, this interaction which this research revealed opens many possibilities for further research in various other aspects of the rail industry. For example, the current industry practice to determine the effectiveness and carry length of friction modifier is to use a tribometer. As it has been revealed both in this research and in others [19] that friction modifier material gets trapped within the surface roughness of the rail and is likely released in elastic deformation as a train wheel passes over it, a tribometer lacks the ability to deform the surface enough to release trapped material and therefore get an accurate reading on the coefficient of friction. Various friction modifier companies will claim its material carries for several miles and the rail industry installs lubricators in accordance with these specifications; however this does not consider the environment, including grade, climate, sand application for traction, contamination of grease, and more.

This prototype is the first which can accurately and repeatedly answer if a rail has detectable material in the field. This study has practical implications for the industry in this regard. The device tested and validated in this study is for stationary spot detection but is portable. Due to its high precision and quasi-static state of the rail, spot checks are adequate to conclude lubricity levels.

Therefore, this study can be summarized into the following significant findings:

1. The detection of thin third-body layers is possible using optical sensors
2. The detection of thin third-body layers can be accurately measured and categorized in a meaningful way to the industry, i.e. “adequate” versus “inadequate.”
3. Optical detection of thin third-body layers is heavily influenced by the roughness of the rail itself
4. The interaction of top-of-rail friction modifiers with the wheel/rail appears to be more of a “seasoning” as this material gets trapped within the surface figure of these solid bodies while the effects of the material remain.
5. Contamination of top-of-rail friction modifier with flange grease is detectable through its fluorescent signature

6.3 Future Studies

The development of this sensor configuration and calculation method is the first step in moving this technology to an industry standard. There are many iterations of this initial design which can close the gap between what has been developed, what the industry is requesting, and what will progress the industry in the future. As what is being detected is not apparent to the human eye or any other measuring device, further calibration can be made by utilizing industry used strain gages which measure lateral forces. Correlating readings at locations with high lateral forces to “clean rail” data will calibrate the prototype to a true unlubricated and unconditioned rail, as high lateral forces are the biggest indicator of a lack of conditioning.

Additionally, the use of optics in this design allow room for the design to move from a stationary prototype to a moving platform. This can be done both at low speeds in the form of a push-cart, and at higher speeds when attached on a hi-rail vehicle. This will allow the rail industry to take these measurements while doing other maintenance in a timely fashion. Graduating to a moving design will need to address issues such as sensitive specular light detection and acquiring a measurement for surface roughness which doesn’t involve cleaning the rail in comparison. This can include a separate study about detecting surface roughness through optical devices and through thin layers.

A few other studies (reference to these studies) and this are beginning to mention the interaction of top-of-rail material and the wheel/rail is much more complicated than a simple third-body, as the surface roughness of the solid wheel/rail influences the degree of third body material which can be trapped and released for another passing train. This “seasoning” effect may change the way top-of-rail friction modifiers are perceived and designed.

References

- [1] M. T. Andani, "The Application of Doppler LIDAR Technology for Rail Inspection and Track Geometry Assessment," Doctor of Philosophy, Mechanical Engineering, Virginia Polytechnic Institute and State University, 2016.
- [2] G. C. S. Kumar, V. Reddy, U. Kumar, "Issues and Challenges with Logistics of Rail Maintenance," presented at the Second International intelligent Logistics Systems Conference, 2006.
- [3] J. C. X. Lu, D.T. Eadie, "Laboratory study of the tribological properties of friction modifier thin films for friction control at the wheel/rail interface," *Wear*, vol. 259, p. 8, 2005.
- [4] M. R. Jan Lundberg, Christina Wanhainen, Johan Casselgren, "Measurements of friction coefficients between rails lubricated with a friction modifier and the wheels of an IORE locomotive during real working conditions," *Wear*, vol. 324-325, p. 9, 2015.
- [5] A. M. Hasan, "Quantitative Laser-based Assessment of Top of Rail Friction Modifiers for Railroad Application," Doctor of Science, Mechanical Engineering, Virginia Polytechnic Institute and State University, 2016.
- [6] K. O. Donald T. Eadie. Dave Elvidge, Richard Stock, Peter Pointner, Joe Kalousek, Peter Klauser, "The effects of top of rail friction modifier on wear and rolling contact fatigue: Full-scale rail-wheel test rig evaluation, analysis and modelling," *Wear*, no. 265, p. 8, 2008.
- [7] D. Plotkin, "Evaluation of a Top-of-Rail Lubrication System," Federal Railroad Administration 2000.
- [8] M. S. D.T. Eadie, "Top-of-rail friction control for curve noise mitigation and corrugation rate reduction," *Journal of Sound and Vibration*, no. 293, p. 10, 2006.
- [9] Y. S. Akira Matsumoto, Hiroyuki Ohno, Masao Tomeoka, Kousuke Matsumoto, Tomohisa Ogino, Masuhisa Tanimoto, Yasushi Oka, Masayuki Okamo, "Improvement of bogie curving performance by using friction modifier to rail/wheel interface," *Wear*, no. 258, p. 9, 2005.
- [10] M. S. Donald T. Eadie, Joe Kalousek, "Railway noise and the effect of top of rail liquid friction modifiers: changes in sound and vibration spectral distributions in curves," *Wear*, no. 258, p. 7, 2005.
- [11] L. Xin, "Study on Determining the Vertical Wheel-Rail Force by Measuring Rail Displacement," presented at the International Conference on Chemical, Material and Food Engineering, 2015.
- [12] F. S. C. Rajpal S. Sirohi, *Optical Methods of Measurement*. New York, 1999, p. 321.
- [13] G. Orellana, "Fluorescence-based sensors," in *Optical Chemical Sensing*, vol. 224, A. N. C. F. Baldini, J. Homola, S. Martellucci, Ed.: Springer, 2006, p. 535.
- [14] R. A. Stone, "Roughness and Relection in Machine Vision," Doctor of Philosophy, Department of Physics, Carnegie-Mellon University, 1994.
- [15] L. M. Jean M. Bennett, *Introduction to Surface Roughness and Scattering*. Washington, D.C.: Optical Society of America, 1989, p. 110.
- [16] T. S. Vorburger, Richard & Brodmann, Rainer & Brodmann, Boris & Seewig, Jörg, "Light Scattering Methods," in *Optical Measurements of Surface Topography*, 2011, pp. 287-311.

- [17] L. J. S. Michael R. Cohen, III. *Diffuse Reflectance Measurements of Standard Diffusers*. Available: <https://www.4physics.com/tn3/lambertian.htm>
- [18] F. J. F. A. Kapoor, S.K. Wong, M. Ishida, "Surface roughness and plastic flow in rail wheel contact," *Wear*, no. 253, p. 8, 2002.
- [19] P. D. Christoph Tomberger, Walter Sextro, Klaus Six, "Friction in wheel-rail contact: A model comprising interfacial fluids, surface roughness, and temperature," *Wear*, no. 271, p. 11, 2011.
- [20] W. Rail, "TOR armor friction modifier product brochure," ed.
- [21] L. B. F. R. Technologies. *Keltrack Trackside Freight Technical Specifications*. Available: http://www.lbfoster-railtechnologies.com/Friction_Modifiers.asp

ACKNOWLEDGEMENTS

The authors wish to thank and acknowledge the US Department of Transportation, University Transportation Center Program (RailTEAM UTC) for funding support for this research.

ABOUT THE AUTHORS

Mehdi Ahmadian, J. Bernard Jones Chair and Director

Dr. Mehdi Ahmadian is a Dan Pletta Professor of Mechanical Engineering at Virginia Tech, where he also holds the position of Director of Center for Vehicle Systems and Safety (CVeSS), and the Railway Technologies Laboratory (RLT). Dr. Ahmadian has authored more than 130 archival journal publications and more than 250 conference publications, including a number of keynote lectures. He has served as Editor or Editor-in-Chief for four journals on Vehicle System Dynamics, Vibration and Control, Shock and Vibration and Automobile Engineering. Dr. Ahmadian is Fellow of American Society of Mechanical Engineers of the American Institute for Aeronautics and Astronautics (AIAA). He has received many distinguished scholar awards.

Dejah Leandra Singh

Ms. Dejah Singh was a graduate research assistant when she worked on this project. She earned a master's degree in mechanical engineering from Virginia Polytechnic Institute and State University, and a bachelor's degree in mechanical engineering from Old Dominion University, Frank Batten College of Engineering and Technology.